DISSERTATION

THE LOCAL CHARACTERISTICS OF INDONESIAN SEAS AND ITS POSSIBLE CONNECTION WITH ENSO AND IOD: TEN YEARS ANALYSIS OF SATELLITE REMOTE SENSING DATA

衛星リモートセンシング観測に基づく最近10年間のインドネシア近海域における海洋環境変動とENSO及びIODとの関係性の解析

September 2013

I DEWA NYOMAN NURWEDA PUTRA

GRADUATE SCHOOL OF SCIENCE AND ENGINEERING
YAMAGUCHI UNIVERSITY JAPAN

ACKNOWLEDGEMENT

First of all writer wish to express sincere gratitude to the Almighty God "Ida Sang Hyang Widhi Wasa" for the blessing so that this dissertation can be finished as one of requirements in the Doctoral Program of Graduate School of Science and Engineering, Yamaguchi University, Japan.

Writer wishes to express sincere gratitude to the thesis supervisor, Prof. Tasuku Tanaka and Prof. Kakuji Ogawara for the inspiring guidance, encouragement, and constructive criticism through course of this work. The deeply grateful for enthusiastic support to Dr. Haruma Ishida who helped us to make our data scientifically sound.

We express our sincere gratitude to DIKNAS and JAXA organizations for the support of our research. We also thank the Remote Sensing Systems for TRMM-TMI and QuikSCAT data; the Earth Observation Research Center, Japan Aerospace Exploration Agency (JAXA EORC) for precipitation data; and the National Oceanic and Atmospheric Administration (NOAA) - Climate Prediction Center (CPC) for ENSO index data; and the Japan Agency for Marine-Earth Science and Technology (JAMSTEC) for IOD index data.

Last but most of all, a very special thanks are extended to my family's, especially my parent, I Dewa Made Putra Tenaya and Desak Nyoman Adnyawati for their sacrifices and understanding, also for my brothers for spending time and grow up together.

August 2013

I Dewa Nyoman Nurweda Putra

CONTENTS

LIST OF TABLES

LIST OF FIGURES

LIST OF ABBREVIATIONS

ABBREVIATIONS

ACF	:	Auto Correlation Function
CERES	:	Clouds and the Earth's Radiant Energy System
Cor.	:	Correlation
ENSO	:	El Nino Southern Oscillation
ETOPO 2	:	Earth Topographic 2
ITF	:	Indonesian Throughflow
IOD	:	Indian Ocean Dipole
LIS	:	Lighting Imaging Sensor
PR	:	Precipitation Radar
RR	:	Rain Rate
SST	:	Sea Surface Temperature
TMI	:	TRMM Microwave Imager
TRMM	:	Tropical Rainfall Measuring Mission
U-WS	:	U (Zonal)-component of Wind Speed
VIRS	:	Visible Infrared Scanner

SYMBOLS

m/s	:	Meter/Second
mm/month	:	Millimeter/Month
km	:	Kilometer

CHAPTER I

INTRODUCTION

1.1 Background

The Indonesian Seas, a semi-closed marginal sea, separates the Pacific Ocean from the Indian Ocean with a chain of big and small islands. The bathymetry is generally shallow (<100 m) throughout the western area of the inner Indonesian Seas, while the abyssal sea basin in the east of the inner Indonesian Seas has the depths of 5000 m. The Indonesian Seas lie on and near the Equator including "warm pool" with its high temperature. The region also has an important pathway for water transport (Gordon *et al.* 2003; Sprintall *et al.* 2004; Gordon *et al.* 2010), the Indonesian throughflow (ITF). ITF affects both the regional circulation and thermal structure (Godfrey 1996).

The general characteristic of the Indonesian seas was reported with the satellite remote-sensing dataset (I Ketut Swardika *et al.* 2012). It concluded that the ocean characteristics, the sea surface temperature (SST), zonal-component of wind speed (U-WS) and rain rate (RR), are very stable in the Equatorial areas, while their seasonal variability appears as increasing the latitude in both the north and south hemispheres. The two abnormal ocean phenomena have been studied since the 1990s: the El Nino-Southern Oscillation (ENSO) and the Indian Ocean Dipole (IOD). ENSO is the anomaly of the wide weather system including ocean, atmosphere and land. Its indicator, or the ENSO index, is the SST in the central tropical Pacific Ocean (Trenberth *et al.* 1998; Diaz *et al.* 2001). IOD is the similar

phenomenon as ENSO and its indicator is the SST difference between the eastern and western tropical Indian Ocean (Saji and Yamagata 2003). It is of great interest whether the ENSO and IOD affect the local characteristics of the Indonesian Seas.

1.2 Problems Formulation

The problems of this research can be formulated as:

1. How are the ocean characteristics and the temporal variability of ocean characters for the local areas in the Indonesian Seas?
2. How is the comparison of those temporal variabilities with the ENSO and IOD indices?
3. How is the influence of the ENSO and IOD phenomena to the Indonesian Seas?
4. How are the local characteristics and the relationship of indices in the Indonesian Seas?

1.3 Objectives

The objectives of this research are to study the local characteristics of the Indonesian Seas including:

1. To analyze the ocean characteristics and to show the temporal variability of ocean characters for the local areas in the Indonesian Seas.
2. To compare those temporal variabilities with the ENSO and IOD indices
3. To consider the influence the ENSO and IOD phenomena to the Indonesian Seas.
4. To show the locality of those variabilities and the correlation of indices.

1.4 Benefits of the Research

Results of this research give benefits such as:

1. Give better knowledge and understanding of ocean character for the local areas in the Indonesian Seas.
2. Can be used as reference for the investigation of the temporal variabilities in the Indonesian Seas and their connection with the ENSO and IOD phenomena.

CHAPTER II

LITERATURE REVIEW

2.1 Tropical Rainfall Measuring Mission (TRMM)

TRMM is the first space mission dedicated to measuring tropical and subtropical rainfall through microwave and visible (infrared) sensors, including the first space borne rain radar (JAXA 2006). The TRMM satellite has 5 sensors on board (see Figure 2.1), which are Precipitation Radar (PR), TRMM Microwave Imager (TMI), Visible Infrared Scanner (VIRS), Clouds and the Earth's Radiant Energy System (CERES), and Lighting Imaging Sensor (LIS) (JAXA 2007).

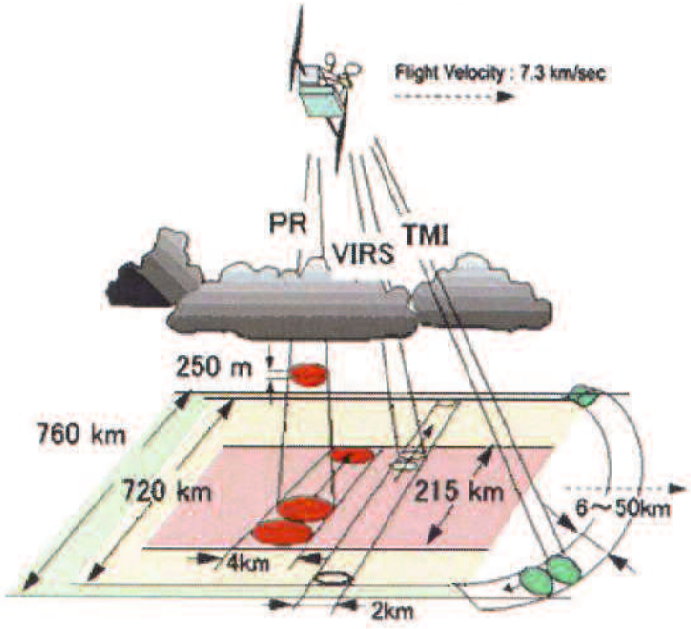

Figure 2.1. Mechanism of TRMM Observation (JAXA 2007)

2.1.1 Precipitation Radar (PR)

The Precipitation Radar (PR) is the primary instrument onboard TRMM. The major objectives of the PR instrument are to provide a 3-dimensional rainfall

structure and to achieve quantitative measurements of the rain rates over both land and ocean (JAXA 2006). The PR system parameters can be described in Table 2.1.

Table 2.1 PR system parameters (JAXA 2006)

Radar Type	Active Phased-array Radar
Frequency	13.796 GHz and 13.802 GHz (Two-channel frequency agility)
Swath Width	~215 Km
Observable Range	From surface to height ≥ 15 Km
Range Resolution	250 m
Horizontal Resolution	4.34±0.12 Km (at nadir)

2.1.2 TRMM Microwave Imager (TMI)

The TRMM Microwave Imager (TMI) is a Multi-channel dual-polarized passive microwave radiometer (JAXA 2006). The TMI system parameters can be described in Table 2.2.

Table 2.2 TMI system parameters (JAXA 2006)

Observation Frequency	10.65, 19.35, 21.3, 37 and 85.5 GHz
Polarization	Vertical / Horizontal (21.3 GHz Channel: Vertical only)
Swath Width	~760 Km
Horizontal Resolution	6 - 50 Km
Scan Mode	Conical Scan (49 deg.)

The measurement of sea-surface temperature (SST) through clouds by satellite microwave radiometers has been an elusive goal for many years. The important feature of microwave retrievals is that SST can be measured through clouds, which are nearly transparent at 10.7 GHz. This is a distinct advantage over the traditional infrared SST observations that require a cloud-free field of view.

Ocean areas with persistent cloud coverage can now be viewed on a daily basis. Furthermore, microwave retrievals are not affected by aerosols and are insensitive to atmospheric water vapor (Remote Sensing System 2009).

2.2 Monsoons

Chung and Siegfried (1994) explained that, the monsoon is basically a response of the atmosphere to the differential heating between the land mass and the adjacent oceans. The atmospheric response, however, may be quite complicated due to the interactions between the atmospheric heat sources, land-sea contrast, and topography. Monsoon is a seasonal prevailing wind which lasts for several months (American Meteorological Society Glossary of Meteorology 2008).

For a seasonal scale, Indonesia has two yearly seasons of monsoon winds, the southeast (dry) monsoon and the northwest (rain) monsoon (Teresa 2008). The seasonal movement of the Inter-tropical Convergence Zone across the equator causes differences in air pressure between the Asian continent and Australia that shift every 6 months and cause a seasonal reversal of the monsoon winds over Indonesia (Pages 2008). This oscillating seasonal pattern of wind is related to Indonesia's geographical location as an archipelago between two large continents in the equatorial zone (Orangutan Foundation International 2007).

2.3 El Nino Southern Oscillation (ENSO)

The periodic warming and cooling of the southeastern Pacific Ocean is actually related to a phenomenon known as Southern Oscillation (Choudhury 1994). The El Nino is characterized by unusually warm ocean temperatures in the

Equatorial Pacific, as opposed to La Nina, which characterized by unusually cold ocean temperatures in the Equatorial Pacific (Tropical Atmosphere Ocean 2013).

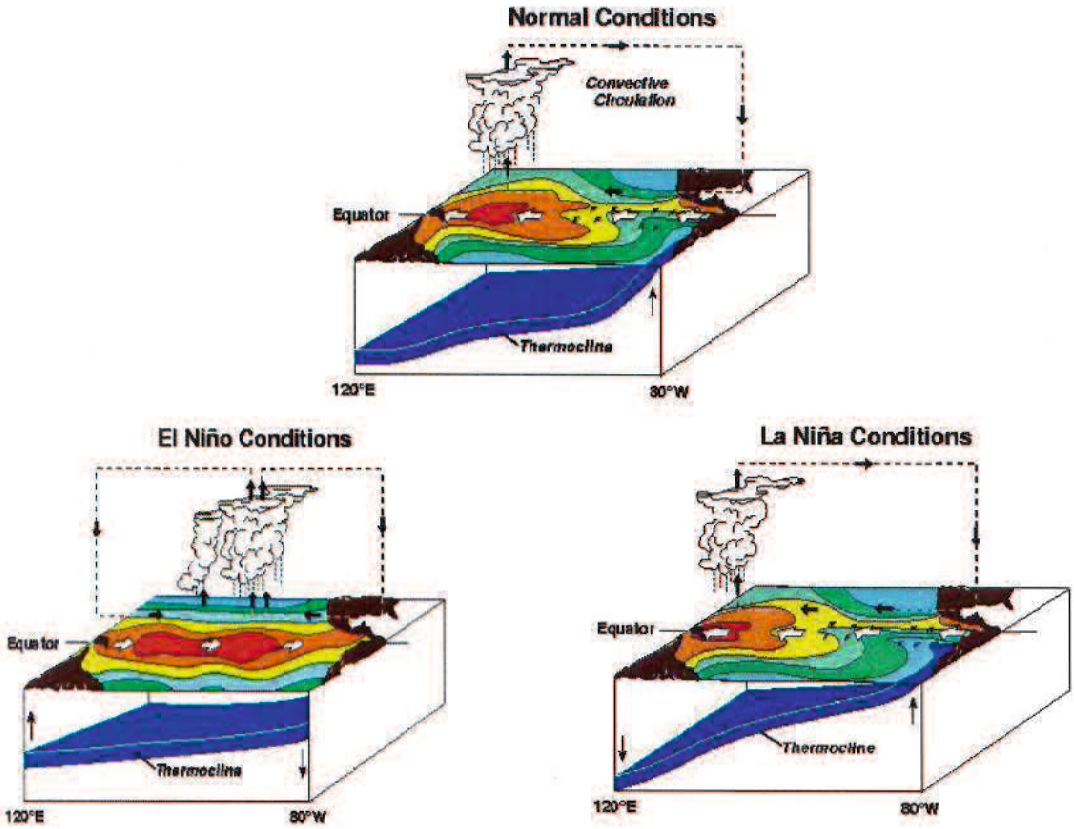

Figure 2.2 Mechanism of ENSO (NOAA 2013)

The Figure 2.2 shows a schematic view of the links between sea-surface temperatures and tropical rainfall (International Research Institute 2013):

a) Normal conditions: The warmest water is found in the western Pacific, as is the greatest rainfall. Winds near the ocean surface travel from east to west across the Pacific (these winds are called *easterlies*).

b) El Nino conditions: The easterlies weaken, warmer than average sea surface temperatures cover the central and eastern tropical Pacific, and the region of heaviest rainfall moves eastward as well.

c) La Nina conditions: Could be thought of as an enhancement of normal conditions. During these events, the easterlies strengthen, colder than average ocean water extends westward to the central Pacific, and the warmer than average sea-surface temperatures in the western Pacific are accompanied by heavier than usual rainfall.

2.4 Indian Ocean Dipole (IOD)

The Indian Ocean Dipole (IOD) is a coupled ocean-atmosphere phenomenon in the Indian Ocean. It is normally characterized by anomalous cooling of SST in the south eastern equatorial Indian Ocean and anomalous warming of SST in the western equatorial Indian Ocean. Associated with these changes the normal convection situated over the eastern Indian Ocean warm pool shifts to the west and brings heavy rainfall over the east Africa and severe droughts/forest fires over the Indonesian region (JAMSTEC 2012).

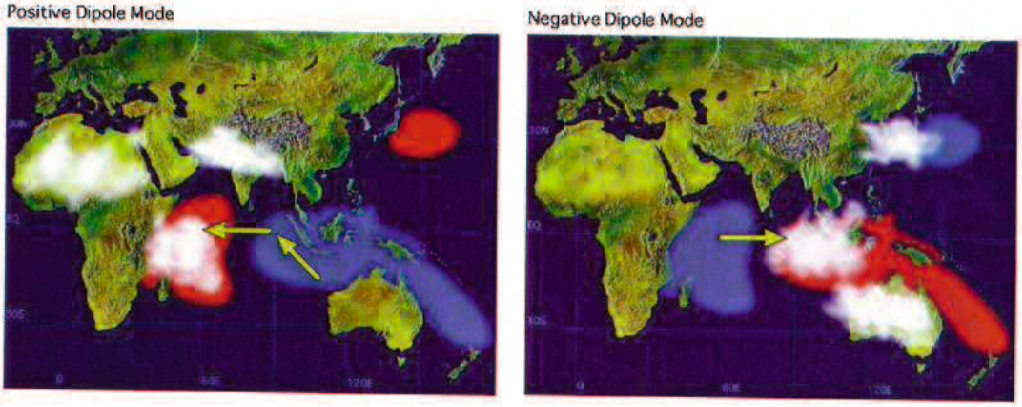

Figure 2.3 Mechanism of IOD (JAMSTEC 2012). SST anomalies are shaded (red color is for warm anomalies and blue is for cold). White patches indicate increased convective activities and arrows indicate anomalous wind directions during IOD events.

CHAPTER III

RESEARCH METHODS

3.1 Research Scheme

The scheme of this research is described in detail in Figure 3.1. This research was begun by collecting the satellite remote sensing dataset and the ENSO and IOD indices for the data processing and finally gives information about the local characteristics of the Indonesian Seas.

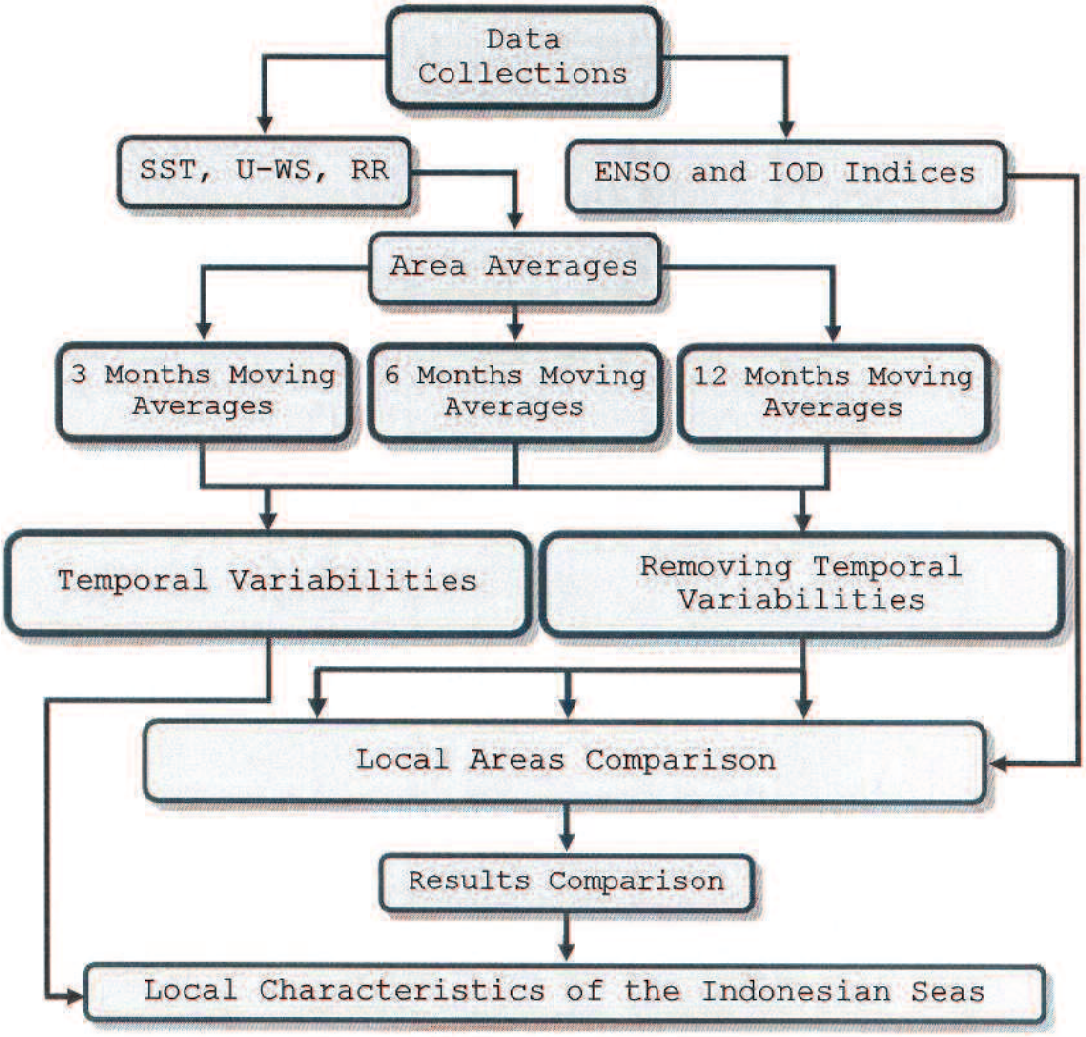

Figure 3.1 Research Scheme

3.2 Data Analyses

We reveal the ocean characteristics from the monthly SST, U-WS and RR in 10 years (December 1999 – November 2009) by satellites observation. Those three data show the clear cyclic variability of the ocean characteristics (I Ketut Swardika *et al.* 2012).

To determine the local variability, we calculate the average of the indices over each local area from the monthly grid data, which is downloaded from the satellite data archives. In order to analyse the temporal variability of indices in the Indonesian Seas, we need to take account of the 6 months variability because the solar looking angle becomes at zenith twice a year.

To detect the seasonal variability, we calculate the 6 months moving averages in which no 6 months variability appears. If there exists a longer than 12 months cyclic variability, it appears in the 12 months moving averages. We should know whether those longer cyclic variabilities exist. Thus we calculate the 6 and 12 months moving averages.

To detect the 6 months variability, we calculate the 3 months moving averages. If a seasonal variability exists, it also appears in the 6 months moving averages. But we can distinguish the 6 months variability from the seasonal variability by carefully expecting the average.

The moving averages for the month-i are calculated as follows:

$$x_i = original\ monthly\ dataset \quad ; i = 1,2,3,\ldots,120 \tag{1}$$

$$X_i = \frac{1}{12}\left[\sum_{j=-5}^{5} x_{i+j} + \frac{1}{2}(x_{i-6} + x_{i+6})\right] \quad ; i = 7,8,9,\ldots,114 \tag{2}$$

$$Y_i = \frac{1}{6}\left[\sum_{j=-2}^{2} x_{i+j} + \frac{1}{2}(x_{i-3} + x_{i+3})\right] \quad ; i = 4,5,6,\ldots,117 \tag{3}$$

$$Z_i = \frac{1}{3}\left[\sum_{j=-1}^{1} x_{i+j}\right] \quad ; i = 2,3,4,\ldots,119 \tag{4}$$

where x_i is the original monthly data and X_i, Y_i, Z_i are the monthly data of the moving averages with 12 months, 6 months and 3 months of length, respectively. The value of X_i, Y_i, Z_i corresponds to the middle of the month.

The ENSO index is defined with the 3 months moving averages of SST in the central tropical Pacific Ocean. If we compare the indices in the Indonesian Seas with the ENSO index, we should take account of both 6 months and seasonal variabilities. As we will show later, all the indices in the ENSO Index area have neither 6 months nor seasonal variabilities. For the comparison, we need the indices free from the 6 months and seasonal variabilities. Thus, we define the deseasonalized (r_i) indices for the purpose of excluding the cyclic temporal variability:

$$p_i = x_i - X_i \quad ; i = 7,8,9,\ldots,114 \tag{5}$$

Then we define the monthly data (s_i) that averaged for 9 years:

$$s_i = \begin{cases} \frac{1}{9}\sum_{k=0}^{8} p_{i+k*12} & ; i = 7,8,9,\ldots,12 \\ \frac{1}{9}\sum_{k=1}^{9} p_{i+k*12} & ; i = 1,2,3,\ldots,6 \end{cases} \tag{6}$$

q_i is defined as:

$$q_i = x_i - s_j \quad ; \quad \begin{matrix} i = 7,8,9,\ldots,114 \\ j = i - \left\lfloor \frac{i}{13} \right\rfloor * 12 \end{matrix} \tag{7}$$

Finally, r_i is defined as the 3 months moving averages of q_i:

$$r_i = \frac{1}{3}\left[\sum_{j=-1}^{1} q_{i+j}\right] \qquad ; i = 8,9,10,\ldots,113 \tag{8}$$

The mathematical explanation of r_i is described as follows: first, we assume that each data of x_i is composed by the cyclic temporal variability (c_i) and the other factor (d_i).

$$x_i = c_i + d_i \tag{9}$$

$$X_i = \frac{1}{12}\left[\sum_{j=-5}^{5}(c_{i+j} + d_{i+j}) + \frac{1}{2}(c_{i-6} + d_{i-6} + c_{i+6} + d_{i+6})\right] \tag{10}$$

$$= \frac{1}{12}\left[\sum_{j=-5}^{5}(c_{i+j}) + \frac{1}{2}(c_{i-6} + c_{i+6})\right] + \frac{1}{12}\left[\sum_{j=-5}^{5} d_{i+j} + \frac{1}{2}(d_{i-6} + d_{i+6})\right] \tag{11}$$

$$= \frac{1}{12}\left[\sum_{j=-5}^{5} d_{i+j} + \frac{1}{2}(d_{i-6} + d_{i+6})\right] \tag{12}$$

The first term of equation (11) is vanished, since:

$$\frac{1}{12}\left[\sum_{j=-5}^{5}(c_{i+j}) + \frac{1}{2}(c_{i-6} + c_{i+6})\right] = 0 \tag{13}$$

Using equation (9) and (10.3) to substitute x_i and X_i, respectively, then gives q_i:

$$q_i = x_i - \left(\frac{1}{9}\sum_{k=0}^{8}(x_{i+k*12} - X_{i+k*12})\right) \tag{14}$$

$$= c_i + d_i - \frac{1}{9}\sum_{k=0}^{8} c_{i+k*12} - \frac{1}{9}\sum_{k=1}^{9} d_{i+k*12} + \frac{1}{108}\sum_{k=1}^{9}\left(\sum_{j=-5}^{5} d_{i+j} + \frac{1}{2}(d_{i-6} + d_{i+6})\right) \tag{15}$$

We assume that:

$$c_i \cong \frac{1}{9}\sum_{k=0}^{8} c_{i+k*12} \quad ; \quad \frac{1}{9}\sum_{k=0}^{8} d_{i+k*12} \cong \frac{1}{108}\sum_{k=0}^{8}\left(\sum_{j=-5}^{5} d_{i+j} + \frac{1}{2}(d_{i-6} + d_{i+6})\right) \tag{16}$$

Substitute equation (16) into equation (15), then gives q_i:

$$q_i \cong d_i \tag{17}$$

Then we get r_i:

$$r_i \cong \frac{1}{3}\sum_{j=-1}^{1} q_{i+j} \cong \frac{1}{3}\sum_{j=-1}^{1} d_{i+j} \tag{18}$$

We also calculate the auto-correlation of SST, U-WS and RR in order to analyse the temporal variability of indices. The auto-correlation function (R_{xx}) is expressed as follows:

$$R_{xx}(\tau) = \frac{C_{xx}(\tau)}{\sigma^2} \tag{19}$$

where

$$C_{xx}(\tau) = \frac{1}{N-k}\sum_{i=1}^{(N-k)} [x_i - \bar{x_i}]\,[x_{i+k} - \overline{x_{i+k}}] \qquad ; k = \tau\Delta t \tag{20}$$

$$\bar{x_i} = \frac{1}{N-k}\sum_{i=1}^{N-k} x_i \quad and \quad \overline{x_{i+k}} = \frac{1}{N-k}\sum_{i=(k+1)}^{N} x_i \tag{21}$$

$$\sigma^2 = \frac{1}{N-k}\sum_{i=1}^{N-k} [x_i - \bar{x}]^2 \quad and \quad \bar{x} = \frac{1}{N-k}\sum_{i=1}^{N-k} x_i \tag{22}$$

To identify the relationship among the indices, the cross-correlation is calculated. The cross-correlation (R_{xy}) is expressed as follows:

$$R_{xy}(\tau) = \frac{C_{xy}(\tau)}{\sigma_x \sigma_y} \tag{23}$$

where

$$C_{xy}(\tau) = \frac{1}{N-k}\sum_{i=1}^{(N-k)} [y_i - \bar{y_i}]\,[x_{i+k} - \overline{x_{i+k}}] \qquad ; k = \tau\Delta t \tag{24}$$

$$\bar{y_i} = \frac{1}{N-k}\sum_{i=1}^{N-k} y_i \quad and \quad \overline{x_{i+k}} = \frac{1}{N-k}\sum_{i=(k+1)}^{N} x_i \tag{25}$$

$$\sigma_x{}^2 = \frac{1}{N-k}\sum_{i=1}^{N-k} [x_i - \bar{x}]^2 \quad and \quad \sigma_y{}^2 = \frac{1}{N-k}\sum_{i=1}^{N-k} [y_i - \bar{y}]^2 \tag{26}$$

$$\bar{x} = \frac{1}{N-k}\sum_{i=1}^{N-k} x_i \quad and \quad \bar{y} = \frac{1}{N-k}\sum_{i=1}^{N-k} y_i \tag{27}$$

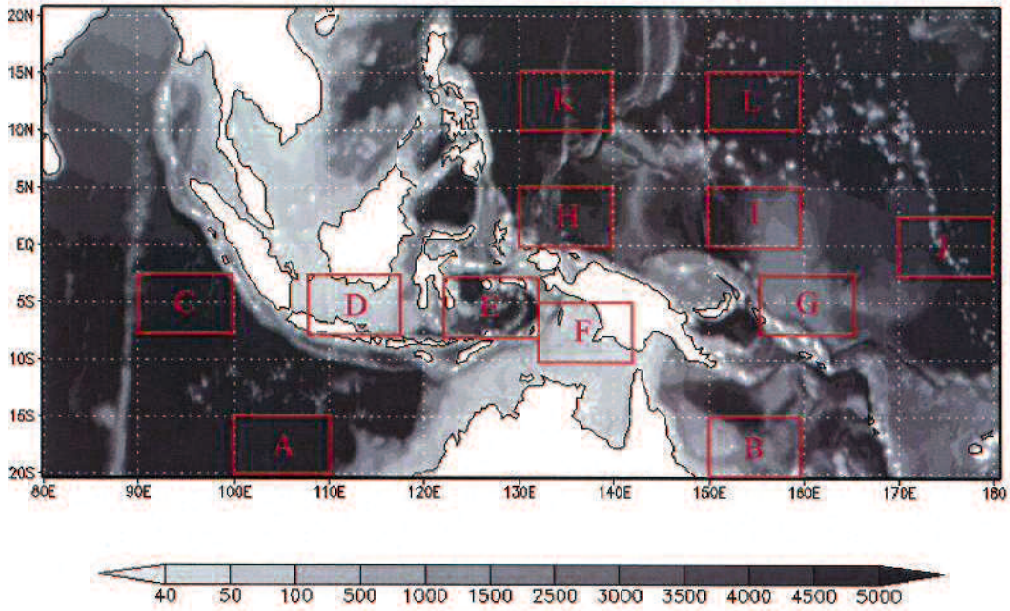

Figure 3.2 The research location and bottom topography map (scale in meter) of the Indonesian Seas derived from ETOPO 2 minutes (Smith and Sandwell 1997). Axes indicate longitude 80° - 180° E and latitude 20° S - 20° N. Areas with shallow water are shaded in light grey, areas with deep water are shaded in dark grey and areas with no available data are in white.

3.3 Research Location

This research was carried out in the Indonesian Seas. We analyzed the whole Indonesian Seas, from 80° - 180° E in longitude and from 20° S - 20° N in latitude (see Figure 3.2), which spans the tropics of both Indian and Pacific Oceans. In order to analyze the local characteristics, the Indonesian Seas is divided into three regions with twelve areas. These three regions represent the south subtropical region, the near-equatorial region and the north subtropical region. The twelve local areas are (see figure 3.2): area A covers the southeast Indian Ocean (100° E - 110° E, 20° S - 15° S); area B covers the southwest Pacific Ocean (150° E - 160° E, 20° S - 15° S); area C covers the Equatorial region of

Indian Ocean (90° E - 100° E, 7° S - 2° S); area D (108° E - 118° E, 7° S - 2° S), area E (122° E - 132° E, 7° S - 2° S) and area F (132° E - 142° E, 10° S - 5° S) cover the inner Indonesian Seas; area G (155° E - 165° E, 7° S - 2° S), area H (130° E - 140° E, 0° - 5° N) and area I (150° E - 160° E, 0° - 5° N) cover the Equatorial region of Pacific Ocean; area J (170° E - 180° E, 3 S° - 3° N) covers the ENSO Index area; area K (130° E - 140° E, 10° N - 15° N) and area L (150° E - 160° E, 10° N - 15° N) cover the northwest Pacific Ocean.

Table 3.1. Specifications of the SST anomaly index.

Index	Area Boundary	Definition
NOAA	5°S-5°N and 160°E-150°W	El Nino: The 3 months moving averages of SST is at least 0.5 warmer than 30-year (1981-2010) average. La Nina: The 3 months moving averages of SST is at least 0.5 cooler than 30-year (1981-2010) average.
JAMSTEC	Western Temperature of Indian Ocean (WTIO): 10°S-10°N and 50°E-70°E South-eastern Temperature of Indian Ocean (SETIO): 10°S-0° and 90°E-110°E (Saji *et al.* 1999)	Positive IOD: The different of WTIO and SETIO is warmer than 30-year (1971-2000) average. Negative IOD: The different of WTIO and SETIO is cooler than 30-year (1971-2000) average.

3.4 Research Materials

We use the monthly data of SST and U-WS that are compiled by the Remote Sensing Systems (REMSS) from TRMM-TMI and QuikSCAT dataset in the 0.25° × 0.25° grid (ftp://ftp.remss.com). The physical dimension of SST and UWS are [deg. Celsius] and [m/s], respectively. For precipitation, we use the TRMM combined level 3 (3B43) versions 6 data, which is compiled and supplied

by the Earth Observation Research Center, Japan Aerospace Exploration Agency (JAXA EORC). The 3B43 version 6 data is recorded monthly in 0.25° grid of horizontal resolution, and its physical dimension is [mm/month].

For the ENSO and IOD phenomena, the ENSO Index and Dipole Mode Index (DMI) are used (see Table 3.1 for the complete definition of the indices). The time series dataset of indices are prepared by NOAA-Climate Prediction Center (CPC) for the ENSO Index dataset and the Japan Agency for Marine-Earth Science and Technology (JAMSTEC) for the DMI dataset.

CHAPTER IV

RESULTS AND DISCUSSION

4.1 Data Processing Results

The 3, 6 and 12 months moving averages for all areas are shown in Figures 4.1 to 4.12. The summaries of the seasonal and 6 months variabilities are presented in Tables 4.1 and 4.2, respectively. The auto-correlation of indices is presented in Table 4.3. The correlation coefficients and time lag among indices are presented in Table 4.4.

The moving averages analysis shows that all indices in area J have neither 6 months nor seasonal variability (see Figures 4.10a-b and 4.30). The ENSO event is defined as the SST which stays for longer than 3 months outside the boundaries ± 0.5 (see Figure 4.24). We summaries the El Nino and La Nina years in Table 4.5 and 4.6, respectively.

The 6 months moving averages of DMI show that the index is affected by the 6 months variability (see Figure 4.25). Thus, in this paper, the abnormal year of IOD is considered only for the year of 2007.

From the all 12 months averages, we observed that there is no longer than 12 months variability, or more precisely, the cyclic variability of longer than 12 months in the Indonesian Seas.

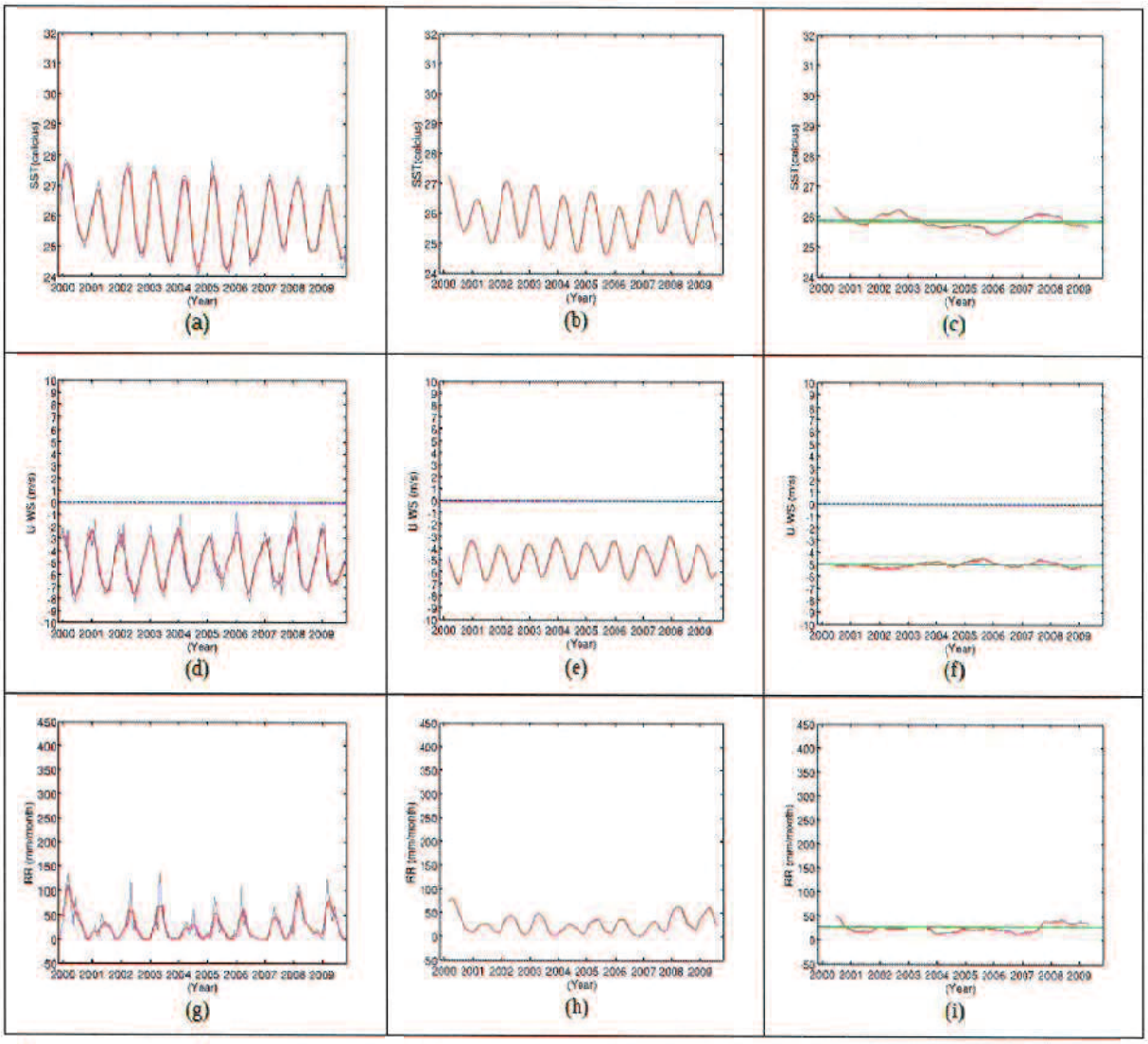

Figure 4.1. Moving averages of SST (upper panel), UWS (middle panel) and RR (lower panel) in area A. The 3 months moving averages are shown in panel (a), (d) and (g); the 6 months moving averages are shown in panel (b), (e) and (h); the 12 months moving averages are shown in panel (c), (f) and (i). The red line indicates the moving averages result, the blue line indicates the original dataset and the green line indicates the average values. Axes indicate averages value of indices and year.

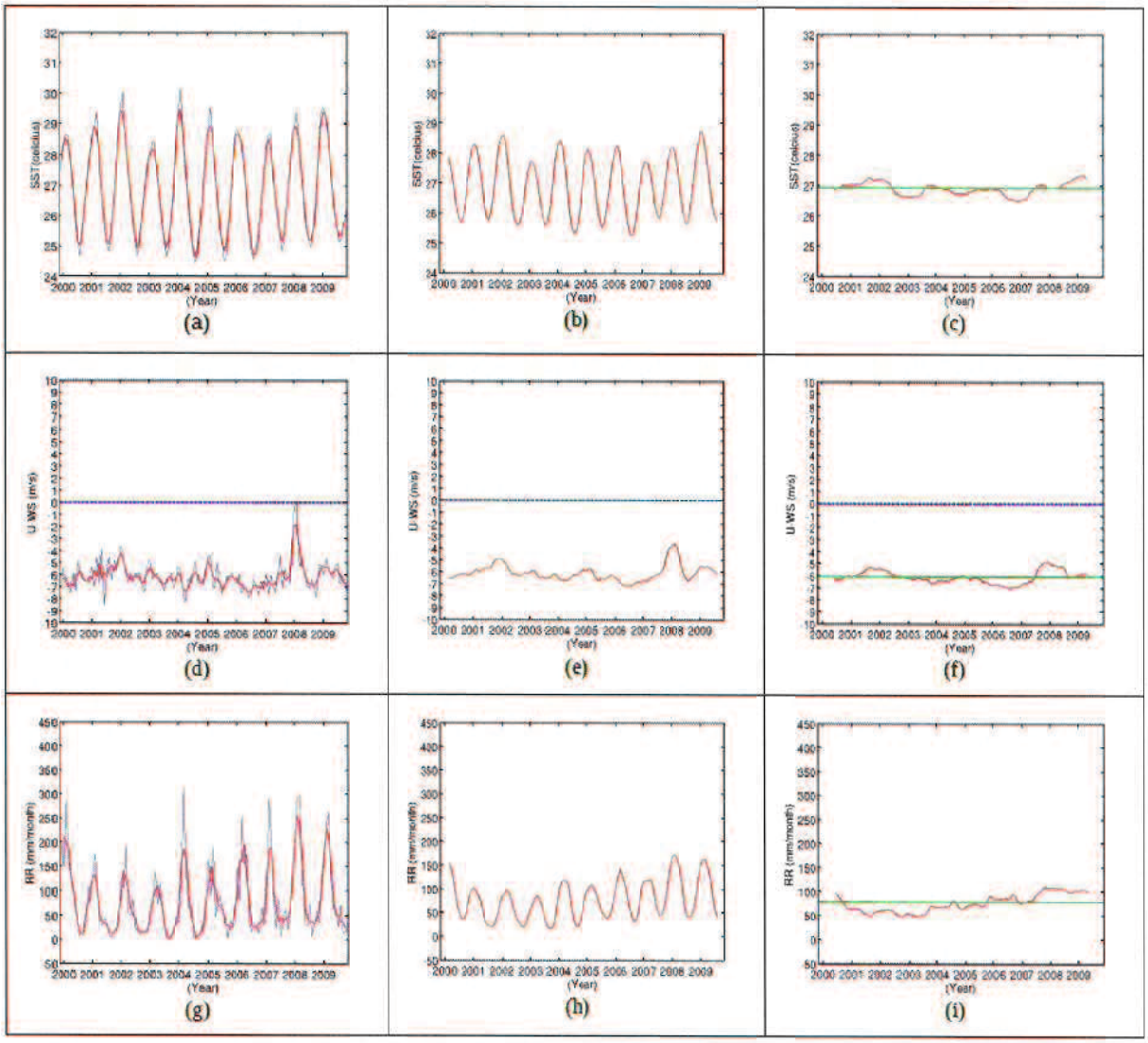

Figure 4.2. Moving averages of SST (upper panel), UWS (middle panel) and RR (lower panel) in area B. The 3 months moving averages are shown in panel (a), (d) and (g); the 6 months moving averages are shown in panel (b), (e) and (h); the 12 months moving averages are shown in panel (c), (f) and (i). The red line indicates the moving averages result, the blue line indicates the original dataset and the green line indicates the average values. Axes indicate averages value of indices and year.

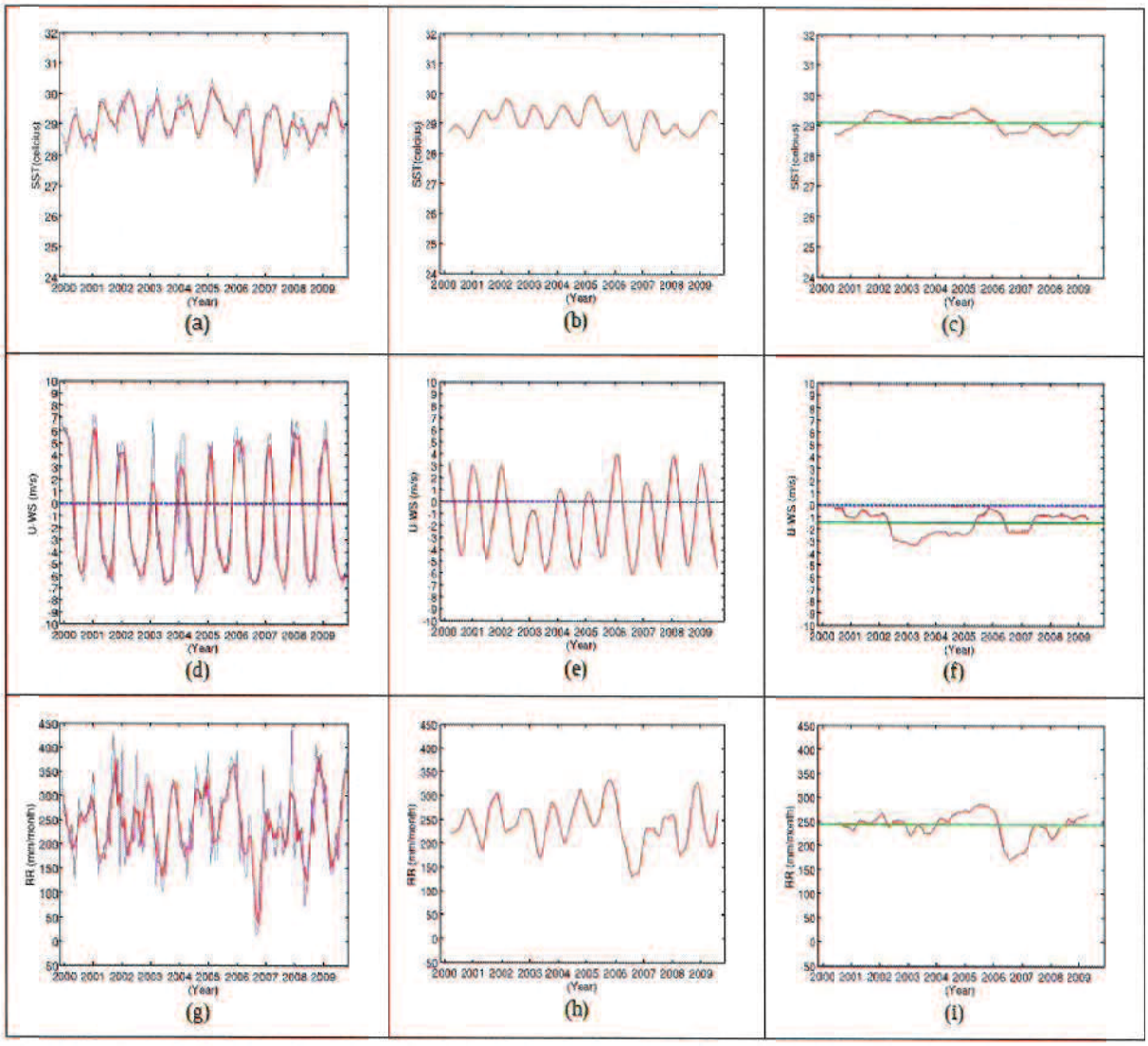

Figure 4.3. Moving averages of SST (upper panel), UWS (middle panel) and RR (lower panel) in area C. The 3 months moving averages are shown in panel (a), (d) and (g); the 6 months moving averages are shown in panel (b), (e) and (h); the 12 months moving averages are shown in panel (c), (f) and (i). The red line indicates the moving averages result, the blue line indicates the original dataset and the green line indicates the average values. Axes indicate averages value of indices and year.

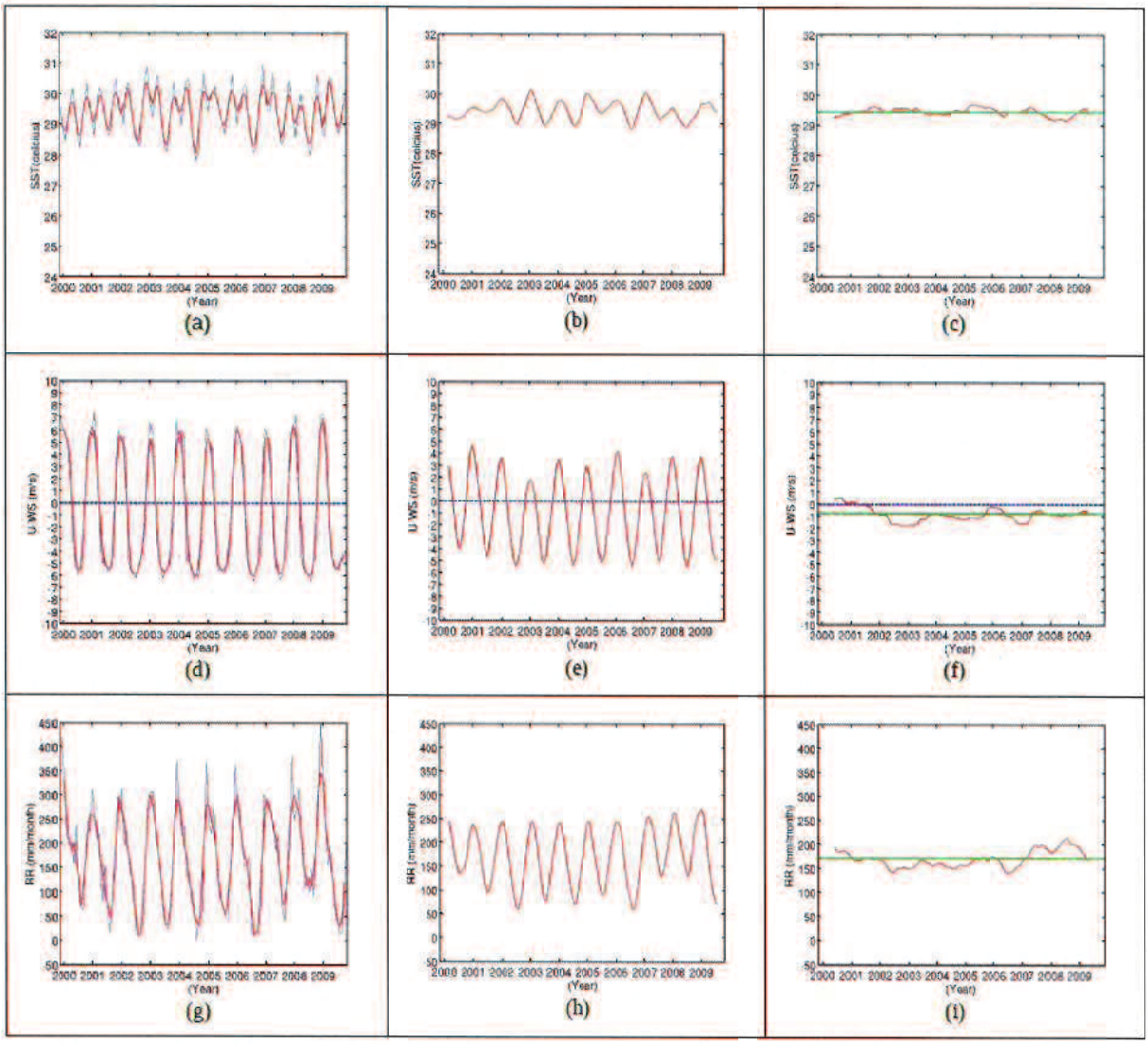

Figure 4.4. Moving averages of SST (upper panel), UWS (middle panel) and RR (lower panel) in area D. The 3 months moving averages are shown in panel (a), (d) and (g); the 6 months moving averages are shown in panel (b), (e) and (h); the 12 months moving averages are shown in panel (c), (f) and (i). The red line indicates the moving averages result, the blue line indicates the original dataset and the green line indicates the average values. Axes indicate averages value of indices and year.

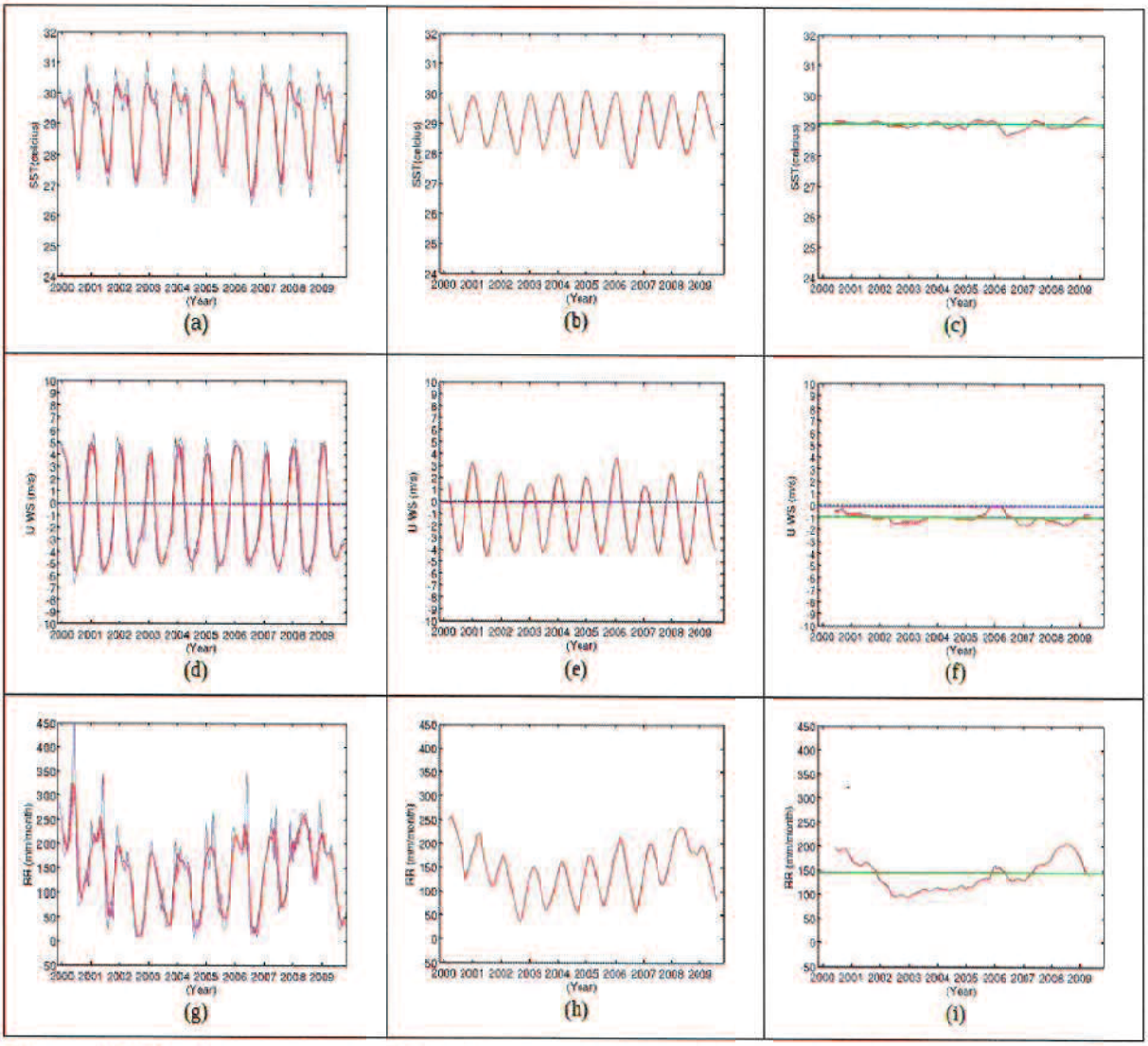

Figure 4.5. Moving averages of SST (upper panel), UWS (middle panel) and RR (lower panel) in area E. The 3 months moving averages are shown in panel (a), (d) and (g); the 6 months moving averages are shown in panel (b), (e) and (h); the 12 months moving averages are shown in panel (c), (f) and (i). The red line indicates the moving averages result, the blue line indicates the original dataset and the green line indicates the average values. Axes indicate averages value of indices and year.

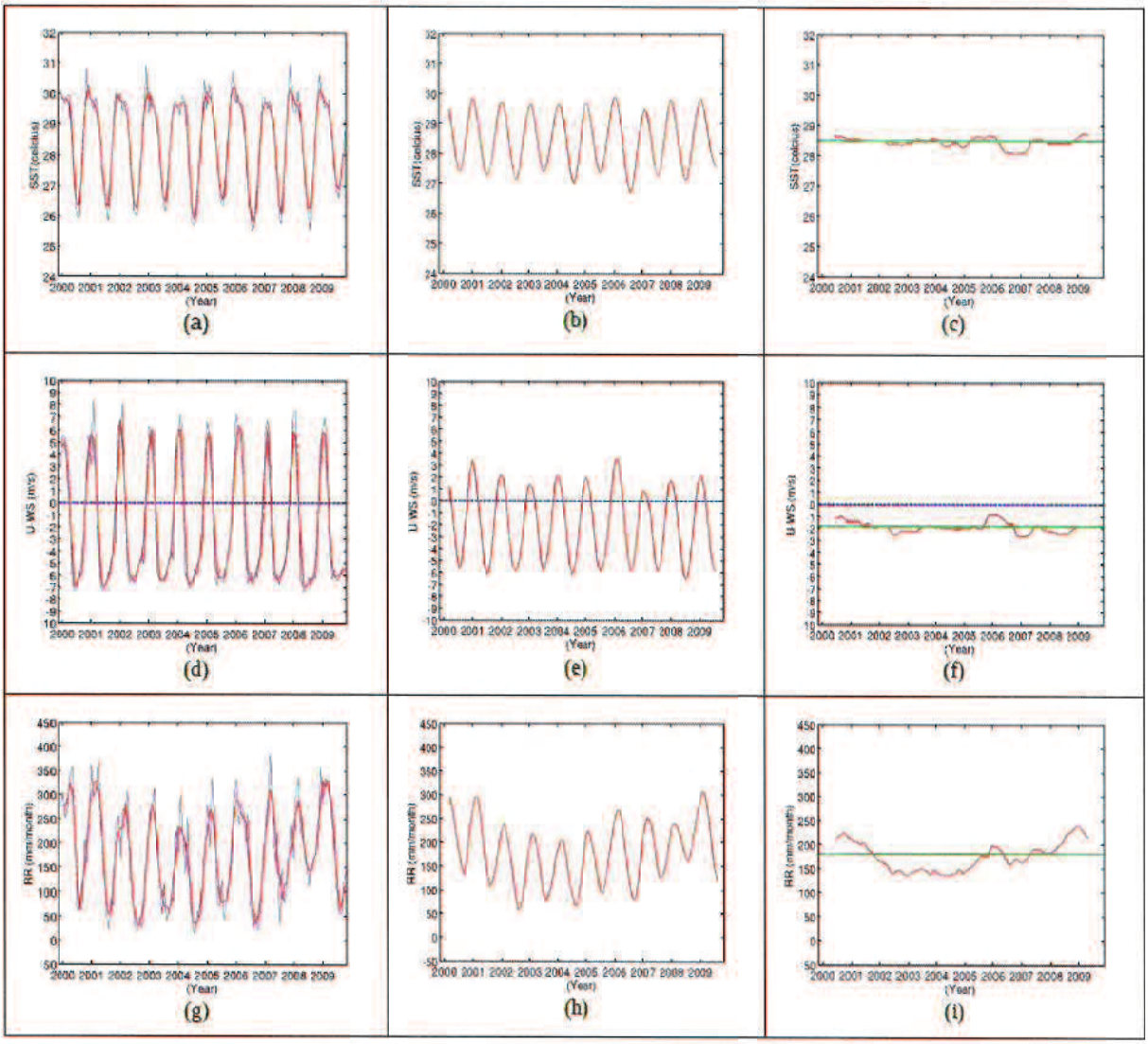

Figure 4.6. Moving averages of SST (upper panel), UWS (middle panel) and RR (lower panel) in area F. The 3 months moving averages are shown in panel (a), (d) and (g); the 6 months moving averages are shown in panel (b), (e) and (h); the 12 months moving averages are shown in panel (c), (f) and (i). The red line indicates the moving averages result, the blue line indicates the original dataset and the green line indicates the average values. Axes indicate averages value of indices and year.

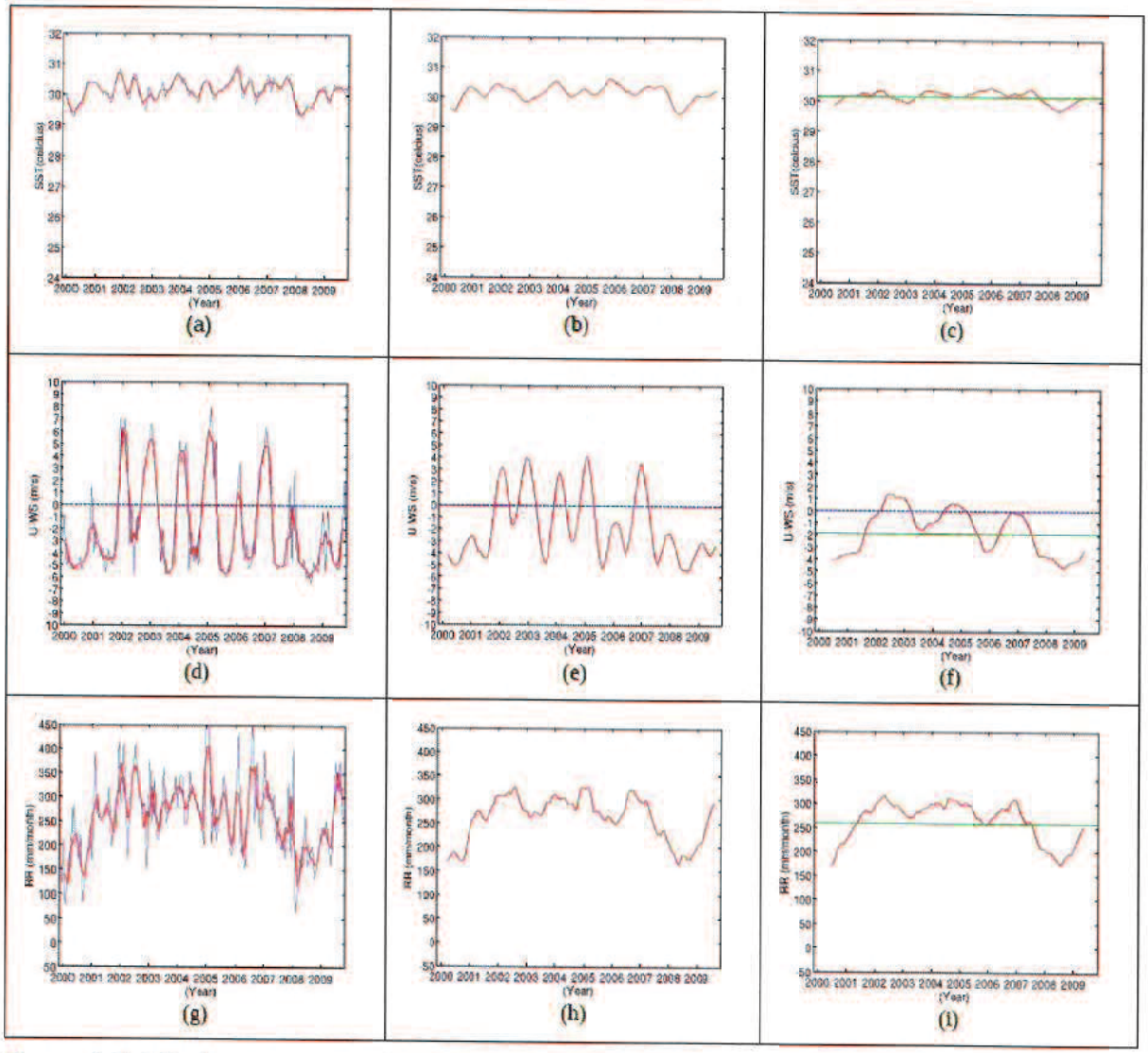

Figure 4.7. Moving averages of SST (upper panel), UWS (middle panel) and RR (lower panel) in area G. The 3 months moving averages are shown in panel (a), (d) and (g); the 6 months moving averages are shown in panel (b), (e) and (h); the 12 months moving averages are shown in panel (c), (f) and (i). The red line indicates the moving averages result, the blue line indicates the original dataset and the green line indicates the average values. Axes indicate averages value of indices and year.

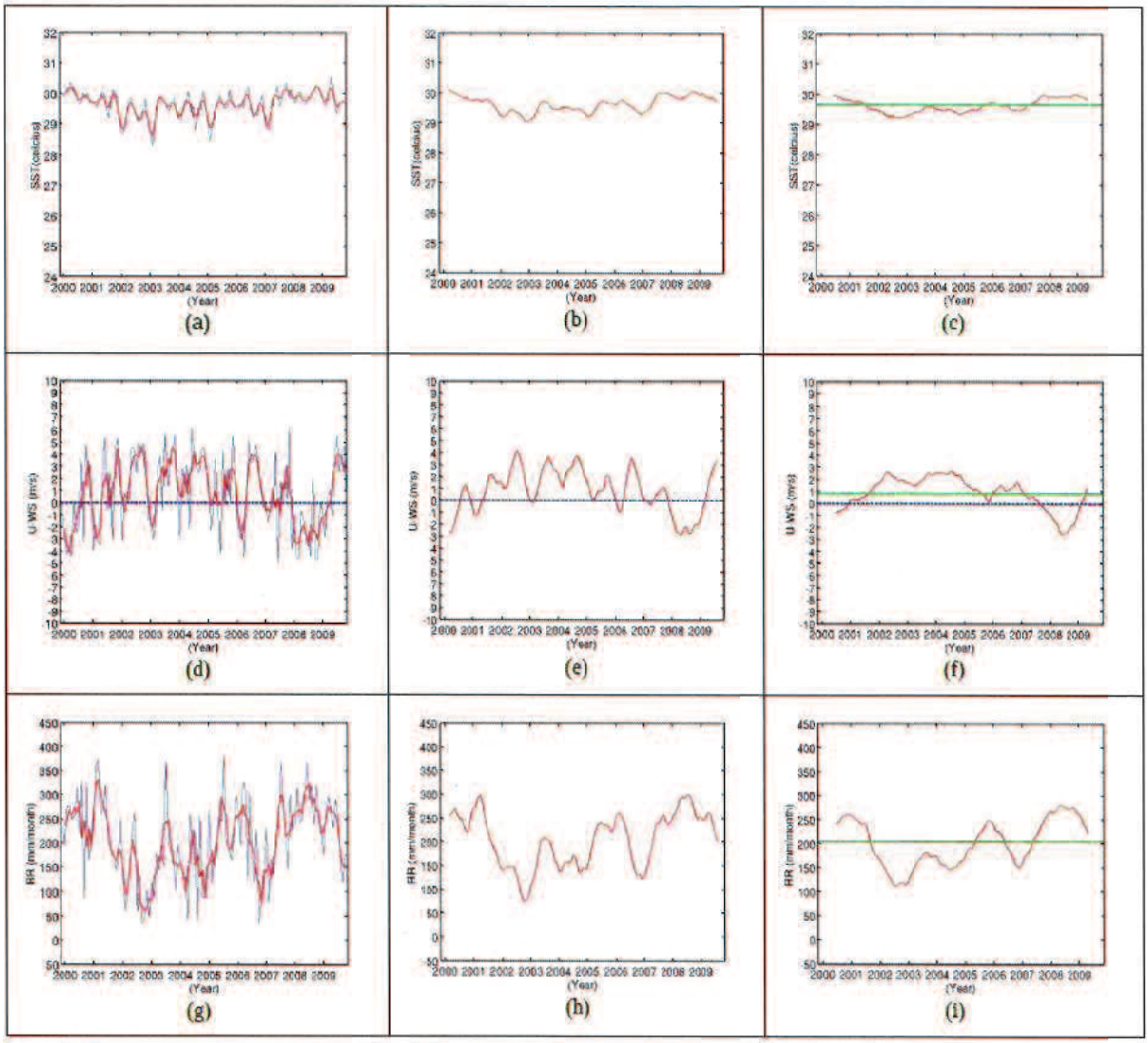

Figure 4.8. Moving averages of SST (upper panel), UWS (middle panel) and RR (lower panel) in area H. The 3 months moving averages are shown in panel (a), (d) and (g); the 6 months moving averages are shown in panel (b), (e) and (h); the 12 months moving averages are shown in panel (c), (f) and (i). The red line indicates the moving averages result, the blue line indicates the original dataset and the green line indicates the average values. Axes indicate averages value of indices and year.

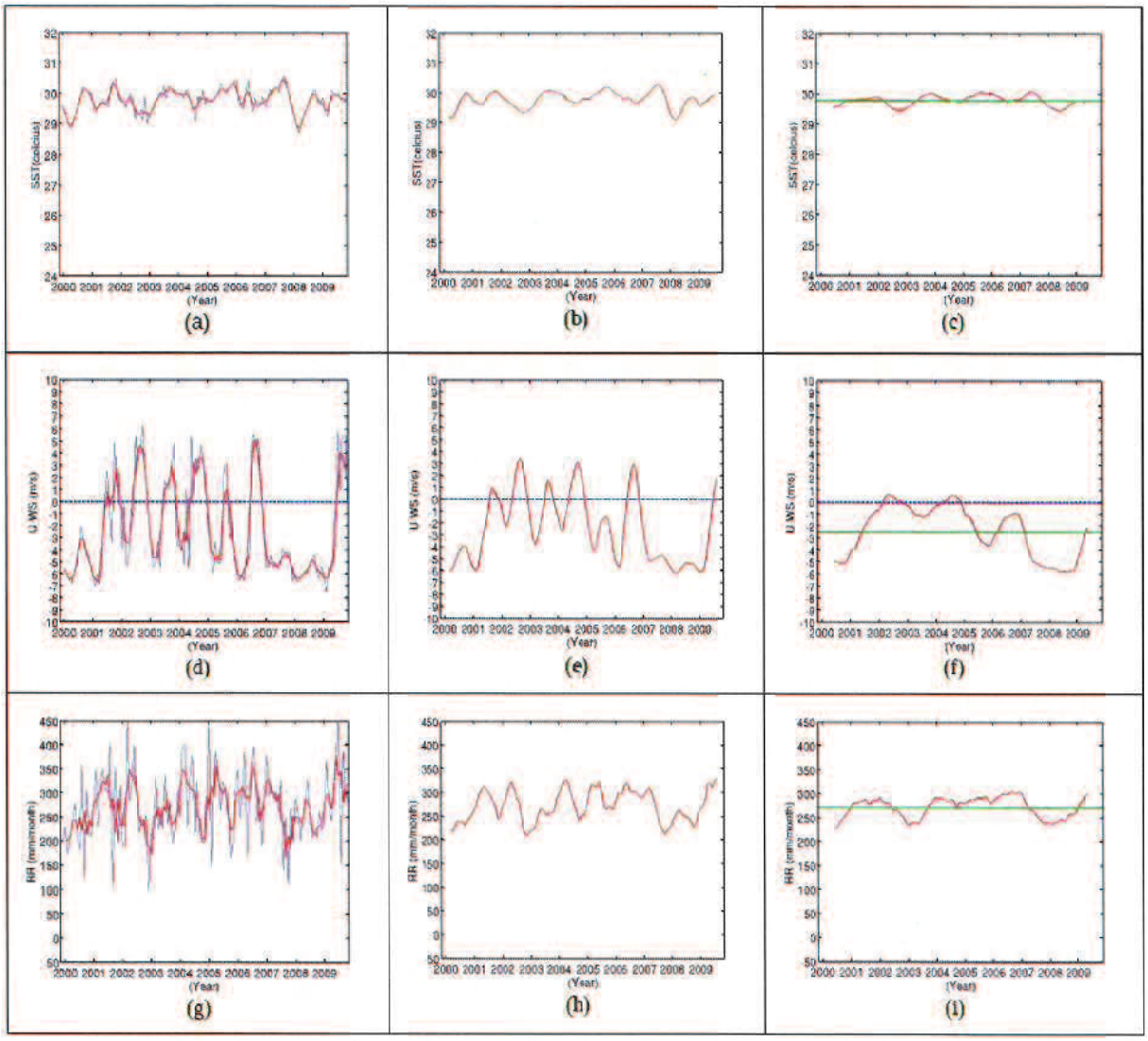

Figure 4.9. Moving averages of SST (upper panel), UWS (middle panel) and RR (lower panel) in area I. The 3 months moving averages are shown in panel (a), (d) and (g); the 6 months moving averages are shown in panel (b), (e) and (h); the 12 months moving averages are shown in panel (c), (f) and (i). The red line indicates the moving averages result, the blue line indicates the original dataset and the green line indicates the average values. Axes indicate averages value of indices and year.

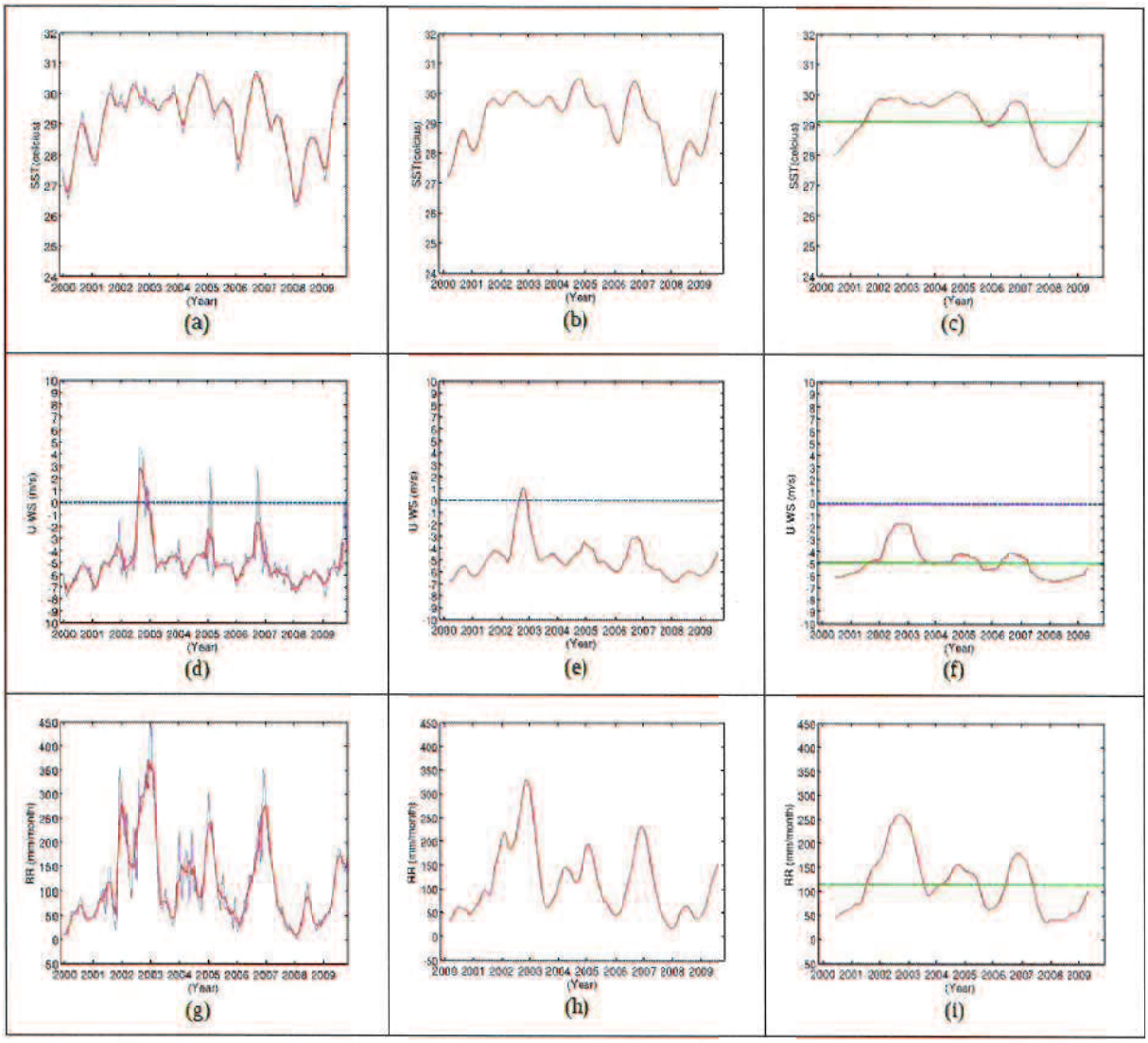

Figure 4.10. Moving averages of SST (upper panel), UWS (middle panel) and RR (lower panel) in area J. The 3 months moving averages are shown in panel (a), (d) and (g); the 6 months moving averages are shown in panel (b), (e) and (h); the 12 months moving averages are shown in panel (c), (f) and (i). The red line indicates the moving averages result, the blue line indicates the original dataset and the green line indicates the average values. Axes indicate averages value of indices and year.

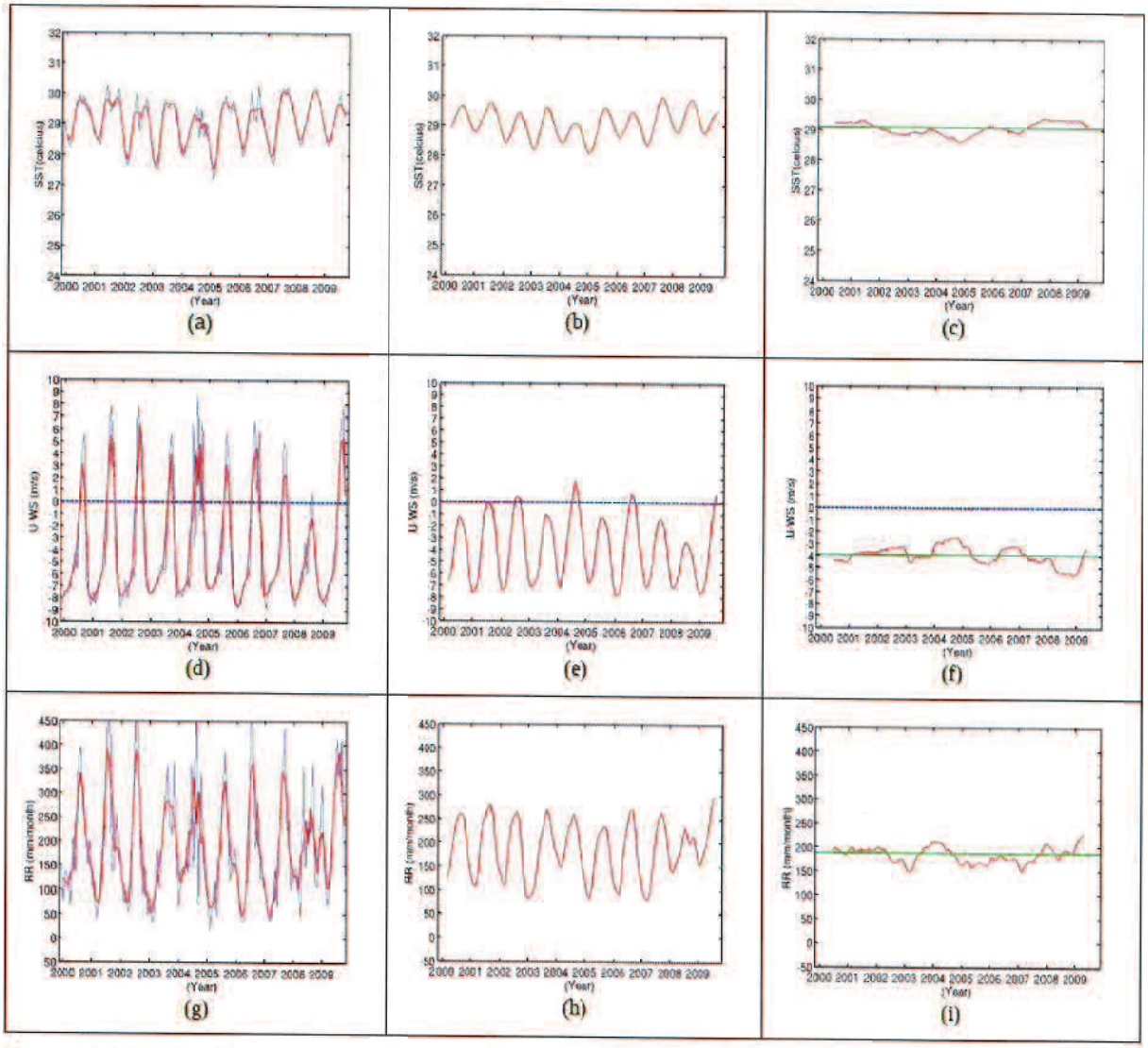

Figure 4.11. Moving averages of SST (upper panel), UWS (middle panel) and RR (lower panel) in area K. The 3 months moving averages are shown in panel (a), (d) and (g); the 6 months moving averages are shown in panel (b), (e) and (h); the 12 months moving averages are shown in panel (c), (f) and (i). The red line indicates the moving averages result, the blue line indicates the original dataset and the green line indicates the average values. Axes indicate averages value of indices and year.

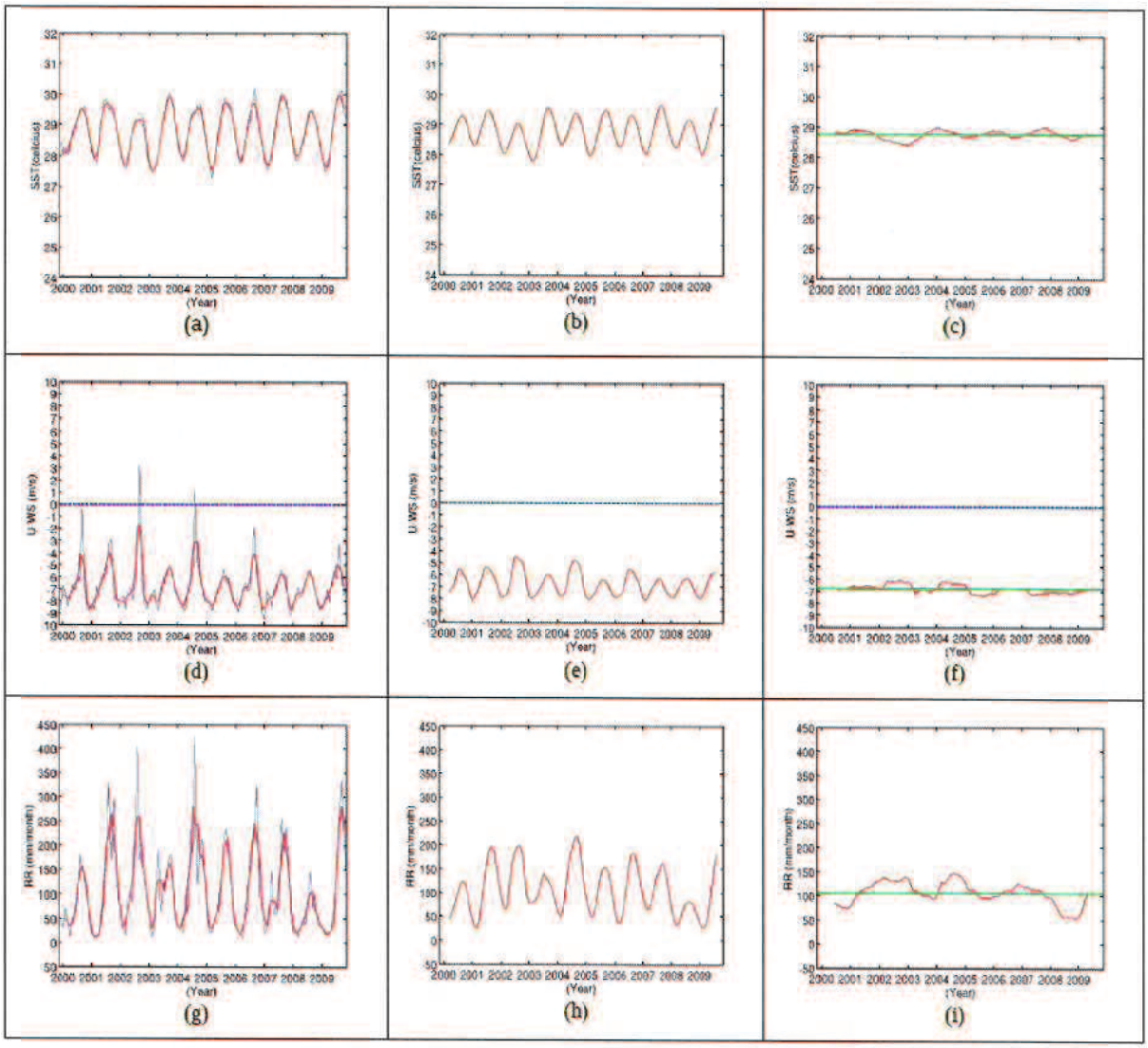

Figure 4.12. Moving averages result of SST (upper panel), UWS (middle panel) and RR (lower panel) in area L. The 3 months moving averages are shown in panel (a), (d) and (g); the 6 months moving averages are shown in panel (b), (e) and (h); the 12 months moving averages are shown in panel (c), (f) and (i). The red line indicates the moving averages result, the blue line indicates the original dataset and the green line indicates the average values. Axes indicate averages value of indices and year.

4.2 The Seasonal Variability

The moving averages are used to analyze the seasonal variability of indices on the local areas of Indonesian Seas. In this research, we categorized the seasonal variability into three types: weak seasonal variability; strong seasonal

variability; and zero seasonal variability, as shown in Figures 4.13, 4.14 and 4.15, respectively. These categories depend on the pattern of moving averages results. It can be shown that the seasonal variability appears in the indices if the patterns of the 6 and 12 months moving averages results are completely different. There also exists a zero seasonal variability of indices if their pattern is similar. Based on these categories, we can determine the seasonal variability of indices on the local areas of Indonesian Seas as shown in Figure 4.16.

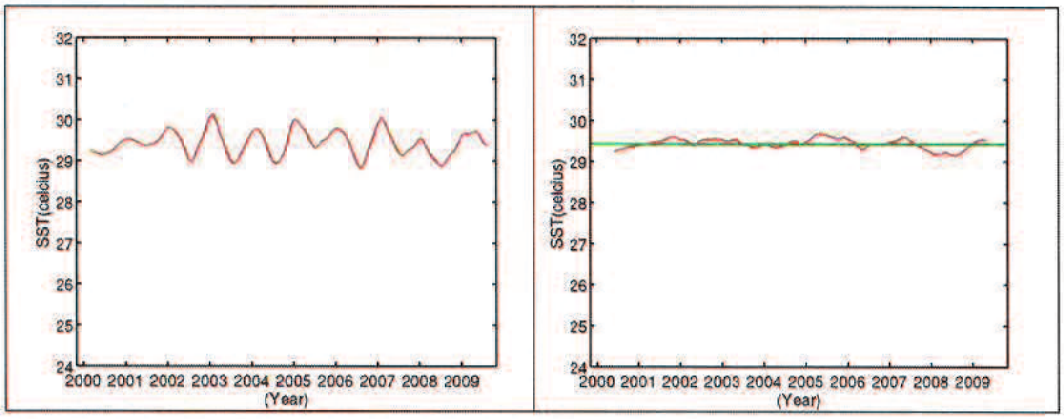

Figure 4.13. Weak seasonal variability. The 6 months moving averages is shown in the left panel; the 12 months moving averages is shown in the right panel. The red line indicates the moving averages result and the green line indicates the average values.

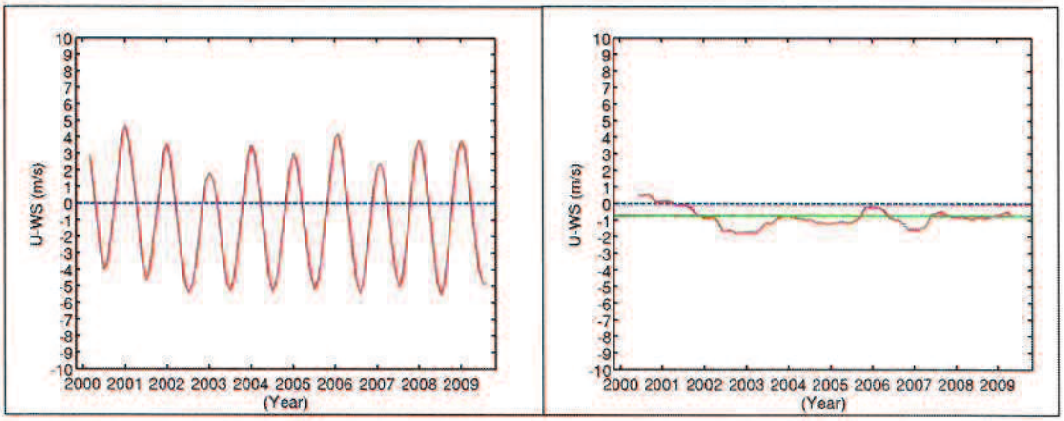

Figure 4.14. Strong seasonal variability. The 6 months moving averages is shown in the left panel; the 12 months moving averages is shown in the right panel. The red line indicates the moving averages result; the blue dot-line indicates the zero value; and the green line indicates the average values.

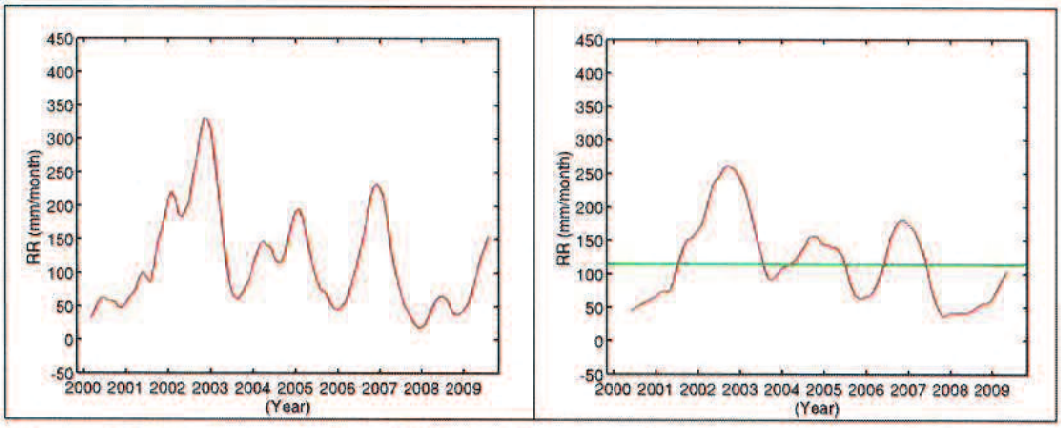

Figure 4.15. Zero seasonal variability. The 6 months moving averages is shown in the left panel; the 12 months moving averages is shown in the right panel. The red line indicates the moving averages result and the green line indicates the average values.

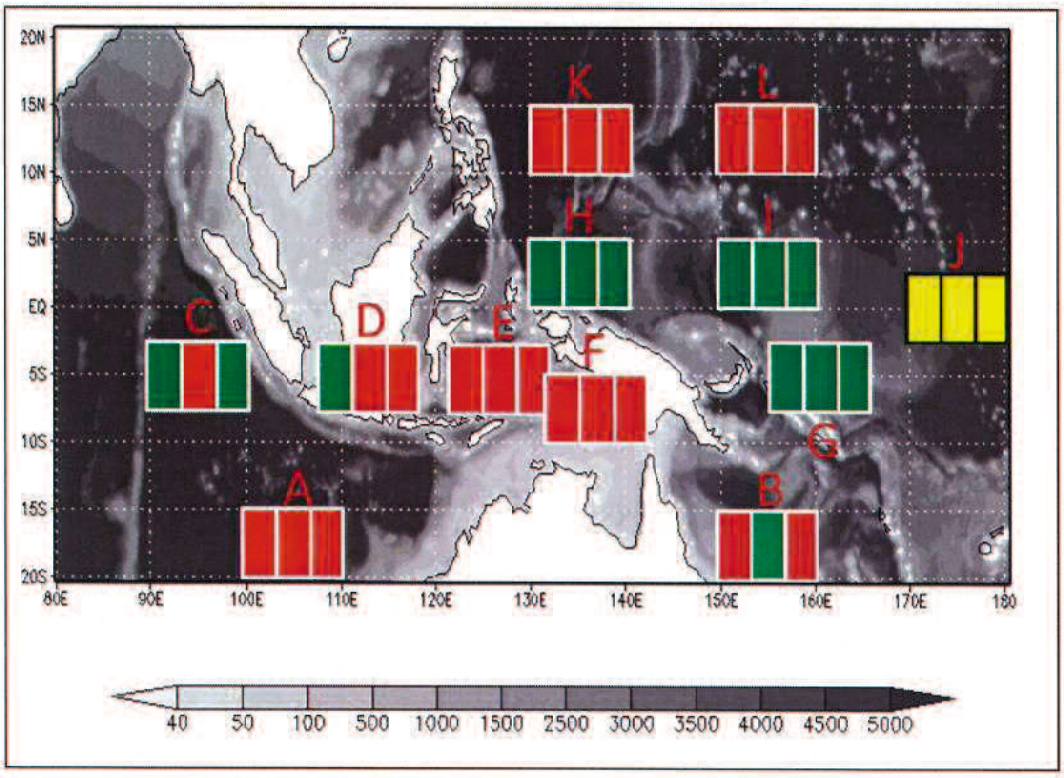

Figure 4.16. The seasonal variability in all local areas. In each local area, the left panel colour indicates the SST variability; the middle panel colour indicates the U-WS variability; the right panel colour indicates the RR variability. The red colour indicates the strong variability; the green colour indicates the weak variability; and the yellow colour indicates the zero variability.

Table 4.1. Seasonal variability of indices

Location	SST	U-WS	RR
Area A	Strong	Strong	Strong
Area B	Strong	Weak	Strong
Area C	Weak	Strong	Weak
Area D	Weak	Strong	Strong
Area E	Strong	Strong	Strong
Area F	Strong	Strong	Strong
Area G	Weak	Weak	Weak
Area H	Weak	Weak	Weak
Area I	Weak	Weak	Weak
Area J	Zero	Zero	Zero
Area K	Strong	Strong	Strong
Area L	Strong	Strong	Strong

4.2.1 The Seasonal Variability of Indices on the Local Areas

The 6 months moving averages of SST, U-WS and RR identify the signal of seasonal variability. Based on Figure 4.16, we made summary for the seasonal variability of indices in Table 4.1. In the High latitude region, all areas show a strong seasonal variability of all indices except for the U-WS in area B. In the Equatorial region, areas D, E and F (the inner Indonesian Seas) shows a strong seasonal variability of all indices except for the SST in area D. The other areas in the Equatorial region show a weak seasonal variability of all indices. It is noted that the ENSO Index area, area J, has no seasonal variability of all indices.

4.3 The 6 Months Variability

The indices in several areas of the Indonesian Seas are affected by the 6 months variability. In this research, we categorized the 6 months variability into three types: weak 6 months variability; very weak 6 months variability; and zero 6 months variability, as shown in Figures 4.17, 4.18 and 4.19, respectively. These

categories depend on the pattern of the moving averages results. It can be shown that the 6 months variability appears in the indices if the patterns of the 3 and 6 months moving averages results are completely different. There also exists zero 6 months variability of indices if their pattern is similar. Based on these categories, we can determine the 6 months variability of indices on the local areas of Indonesian Seas as shown in Figure 4.20.

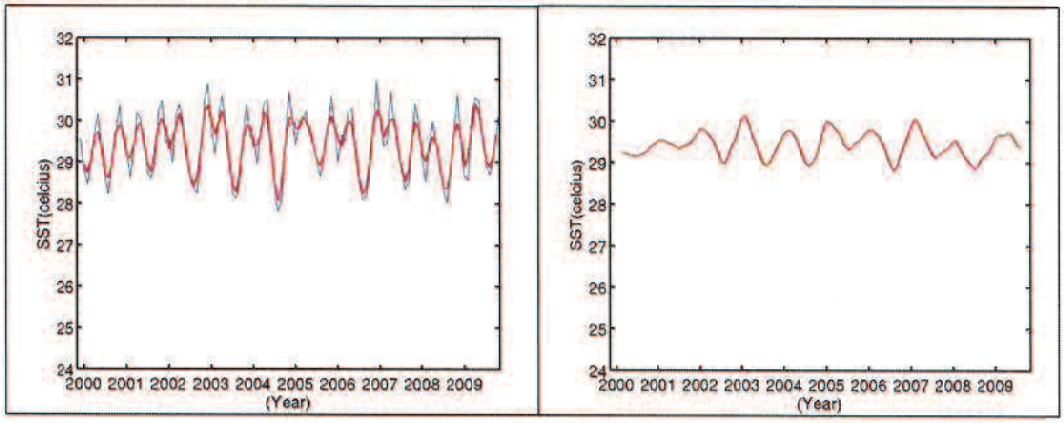

Figure 4.17. Weak 6 months variability. The 3 months moving averages is shown in the left panel; the 6 months moving averages is shown in the right panel. The red line indicates the moving averages result and the blue line indicates the original dataset.

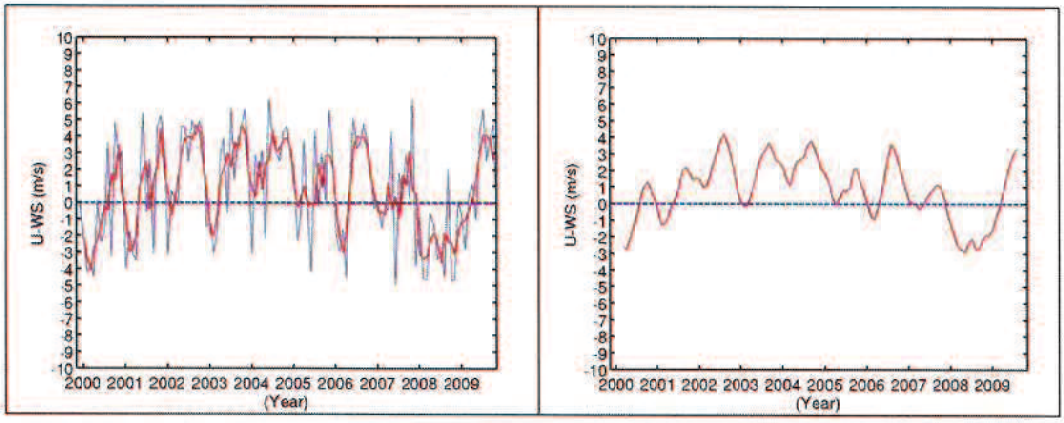

Figure 4.18. Very weak 6 months variability. The 3 months moving averages is shown in the left panel; the 6 months moving averages is shown in the right panel. The red line indicates the moving averages result; the blue line indicates the original dataset; and the blue dot-line indicates the zero value.

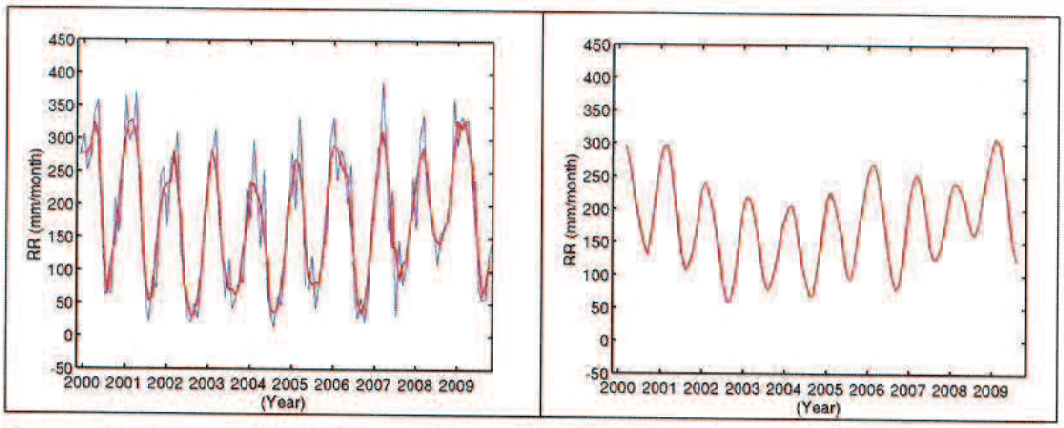

Figure 4.19. Zero 6 months variability. The 3 months moving averages is shown in the left panel; the 6 months moving averages is shown in the right panel. The red line indicates the moving averages result and the blue line indicates the original dataset.

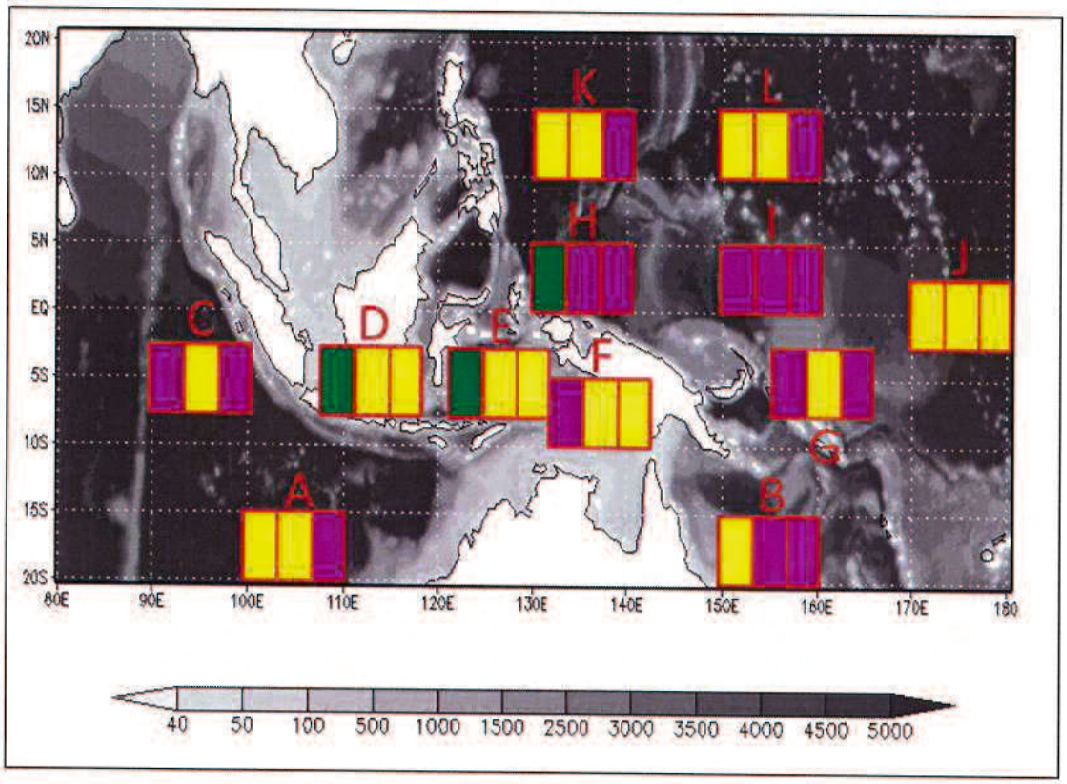

Figure 4.20. The 6 months variability in all local areas. In each local area, the left panel-colour indicates the SST variability; the middle panel-colour indicates the U-WS variability; the right panel-colour indicates the RR variability. The purple colour indicates the very weak variability; the green colour indicates the weak variability; and the yellow colour indicates the zero variability.

Table 4.2. Six months variability of indices

Location	SST	U-WS	RR
Area A	Zero	Zero	Very weak
Area B	Zero	Very weak	Very weak
Area C	Very weak	Zero	Very weak
Area D	Weak	Zero	Zero
Area E	Weak	Zero	Zero
Area F	Very weak	Zero	Zero
Area G	Very weak	Zero	Very weak
Area H	Weak	Very weak	Very weak
Area I	Very weak	Very weak	Very weak
Area J	Zero	Zero	Zero
Area K	Zero	Zero	Very weak
Area L	Zero	Zero	Very weak

4.3.1 The 6 Months Variability of Indices on the Local Areas

The 3 months moving averages of SST, U-WS and RR identify the signal of the 6 months variability. Based on Figure 4.20, we made summary for the 6 months variability of indices in Table 4.2. In the High latitude region, all areas have no 6 months variability of SST and U-WS, except for the area B. The area B shows a very weak 6 months variability of U-WS. All areas in the High latitude region show a very weak 6 months variability of RR.

In the Equatorial region, areas D, E and H show a weak 6 months variability of SST. The other areas in the Equatorial region only show a very weak 6 months variability of SST. The areas H and I show a very weak 6 months variability of U-WS. The other areas in the Equatorial region have no 6 months variability of U-WS. The inner Indonesian Seas, areas D, E and F have no 6 months variability of RR, while the other areas in the Equator show a very weak 6

months variability of RR. It is noted that the ENSO Index area, area J, has no 6 months variability of all indices.

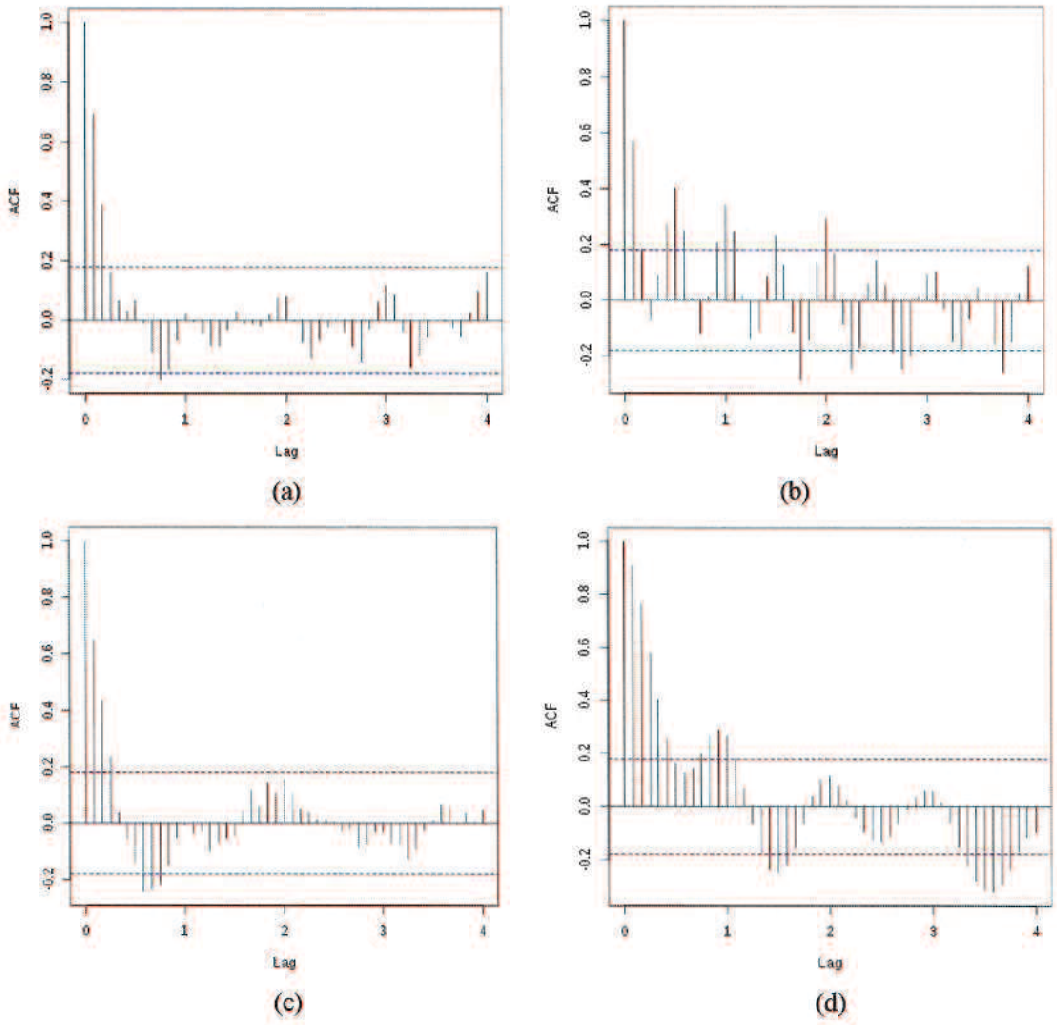

Figure 4.21. The auto-correlation of SST within 4 years in area G (panel a), area H (panel b), area I (panel c) and area J (panel d). Axes indicate correlation value of indices and lag-time.

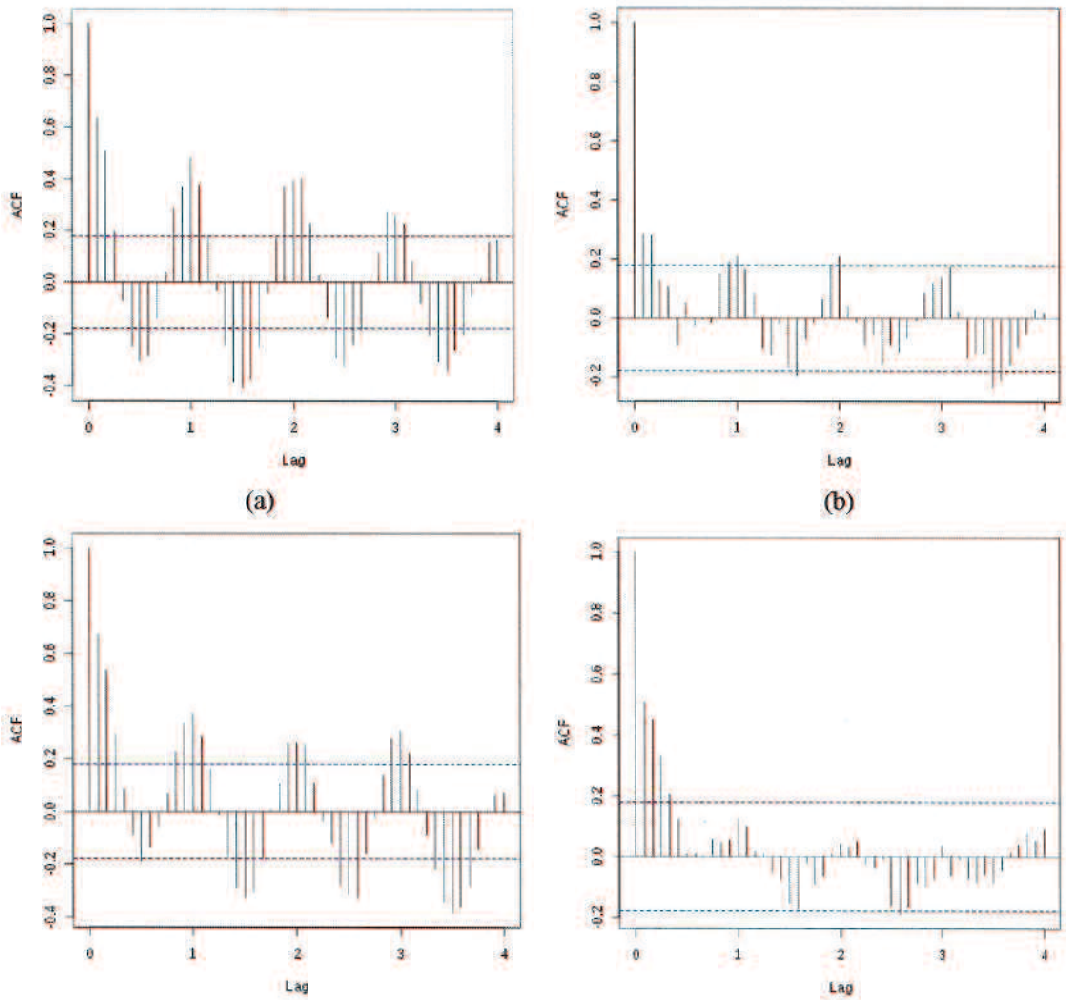

Figure 4.22. The auto-correlation of U-WS within 4 years in area G (panel a), area H (panel b), area I (panel c) and area J (panel d). Axes indicate correlation value of indices and lag-time.

4.4 The Auto-correlation and Cross-correlation Analyses

We further calculate the auto-correlation of SST, U-WS and RR to find out the temporal variability of indices for those areas with a weak seasonal variability: the areas G, H, I and J in the Equatorial Pacific Ocean (see Figures 4.21 to 4.23). These areas (see Table 4.3) have no clear temporal variability of SST and RR, except for areas H. The area H shows combined seasonal and 6 months variability

of SST. The temporal variability of U-WS in all areas shows the seasonal variability, except for the ENSO Index area, area J.

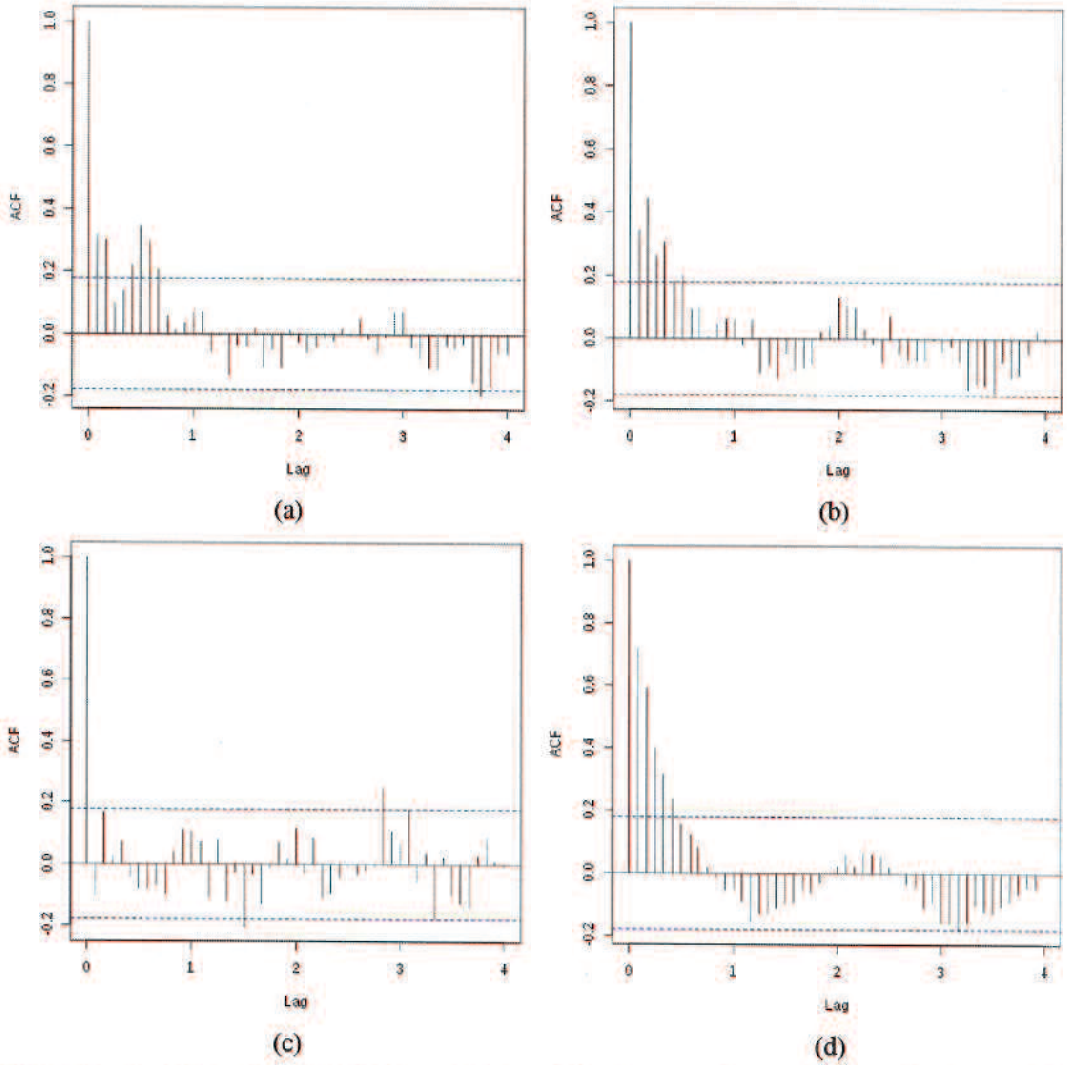

Figure 4.23. The auto-correlation of RR within 4 years in area G (panel a), area H (panel b), area I (panel c) and area J (panel d). Axes indicate correlation value of indices and lag-time.

Table 4.3. Auto-correlation of indices

Location	Variability		
	SST	U-WS	RR
Area G	NC	1 Year	NC
Area H	6 months	1 Year	NC
Area I	NC	1 Year	NC
Area J	NC	NC	NC

The NC symbol indicates the variability is not clear.

We also calculate the cross-correlation among the indices (see Table 4.4). In the High latitude region, all areas show a strong correlation among indices, except for the area B. The lag time of SST and U-WS for area A is -2 months (it means that the SST comes 2 months later after the U-WS), while those for areas K and L are -1 month. The lag times of U-WS and RR for the areas A, K and L are -2, 0 and 1 months, respectively. The lag times of SST and RR for the areas A, K and L are 2, 1 and 0 months, respectively. The area B only shows a strong correlation between SST and RR with 1 month lag time.

Table 4.4. Time-lagged correlation among indices.

Location	SST - UWS		UWS - RR		SST - RR	
	Cor.	Lag (month)	Cor.	Lag (month)	Cor.	Lag (month)
Area A	0.80	-2	0.60	-2	0.71	2
Area B	Very low	-	Very low	-	0.76	1
Area C	-0.53	4	Very low	-	Very low	-
Area D	-0.55	5	0.68	0	0.60	0
Area E	0.66	0	0.59	2	0.74	1
Area F	0.69	0	0.65	1	0.78	1
Area G	Very low	-	Very low	-	Very low	-
Area H	Very low	-	Very low	-	Very low	-
Area I	Very low	-	Very low	-	Very low	-
Area J	0.52	0	0.50	0	0.68	0
Area K	0.50	-1	0.64	0	0.68	1
Area L	0.61	-1	0.56	1	0.76	0

In the Equatorial region, areas D, E and F (the inner Indonesian Seas) show a strong correlation among indices. The lag time of SST and U-WS for area D is 5 months, while those for areas E and F are 0 month. The lag times of U-WS and RR for areas D, E and F are 0, 2 and 1 months, respectively. The lag time of SST and RR for area D is 0 month, while those for areas E and F are 1 month. The

area C only shows a strong correlation between SST and U-WS with 4 months lag times. The ENSO Index area, area J, has no lag time among indices.

4.5 The Connection of Indices with ENSO and IOD

To determine the ENSO and IOD years, we plot the ENSO Index and DMI dataset in Figures 4.24 and 4.25, respectively. As our analyses for the temporal variability of indices on the local areas, the ENSO index area (area J) shows that all indices are free from the cyclic temporal variability, while the indices in the IOD index area (area C) are affected by the cyclic temporal variability. The DMI dataset also shows the 6 months variability (see Figure 4.25). Thus, to find out the original signal of IOD, we remove the 6 months variability from the DMI dataset by the 6 months moving averages. After removing the 6 months variability, we found that the IOD event only occurs in the year of 2007. The analysis of RR in area C (see Figure 4.26) also indicates that the significant response of RR is more correspond to the 6 months moving averages of DMI dataset.

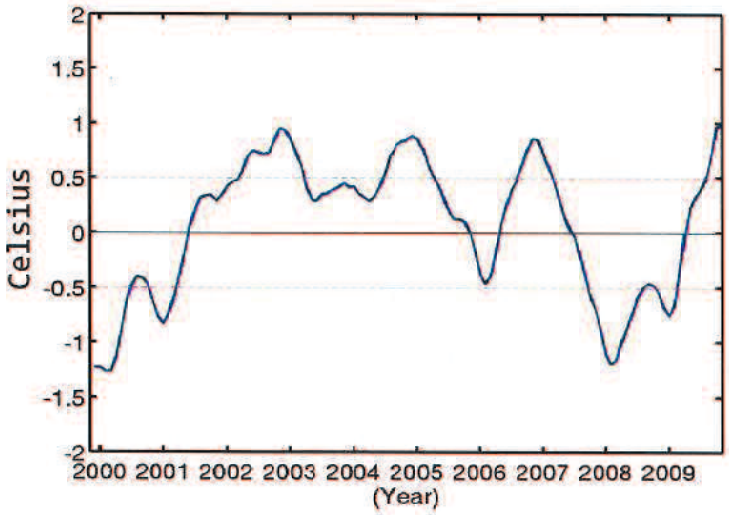

Figure 4.24. ENSO years based on NOAA Index. SST is at least 0.5 warmer than 30-year average indicates the El Nino event. SST is at least 0.5 cooler than 30-year average indicates the La Nina event.

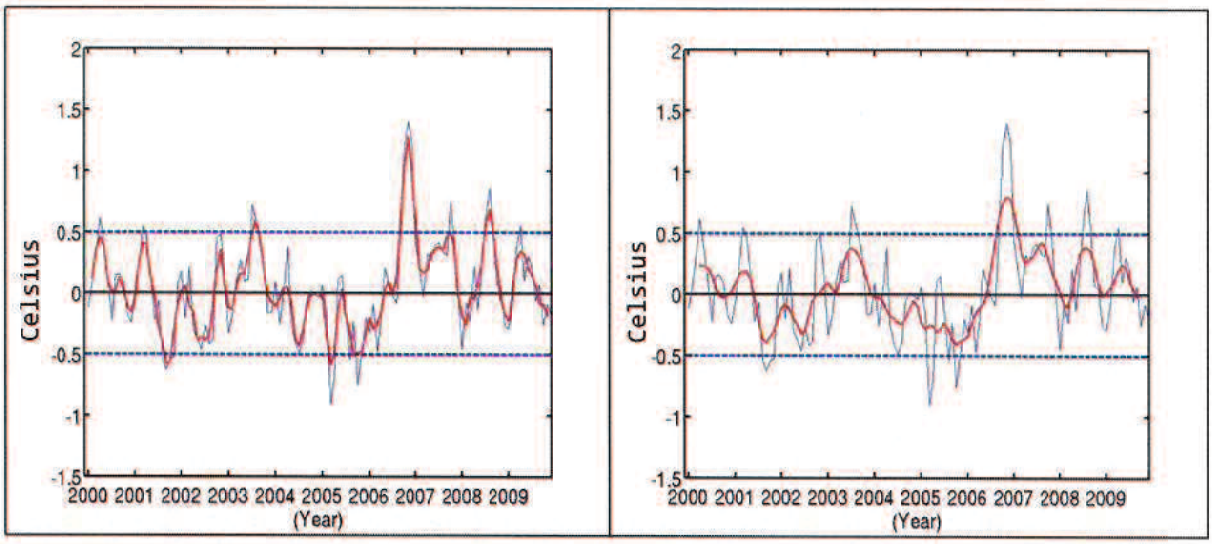

Figure 4.25. The moving averages of DMI dataset. The 3 months moving averages are shown in panel a; the 6 months moving averages are shown in panel b. The red line indicates the moving averages result and the blue line indicates the original dataset. Axes indicate value of index (deg. Celcius) and year.

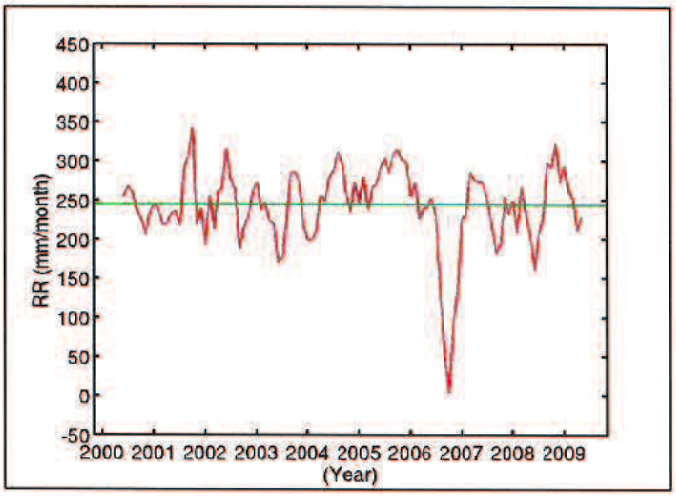

Figure 4.26. The RR response in area C. The red line indicates the moving averages result and the green line indicates the 10 years averages value. Axes indicate averages value of RR (mm/month) and year.

4.5.1 The ENSO and IOD Signals Detection

The temporal variability analyses on the local areas show that the characteristics of indices are easily disturbed by the cyclic temporal variability, except for the ENSO index area (area J). Then, the possible connection of indices with the ENSO and IOD phenomena in the Indonesian Seas are analyzed by

removing the cyclic temporal variability: the variability longer than 12 months; seasonal variability; and the 6 months variability from the indices (see Figure 4.27). This proposed method improves the detection of ENSO and IOD signal especially for the areas that show a cyclic temporal variability in the indices (see Figure 4.28).

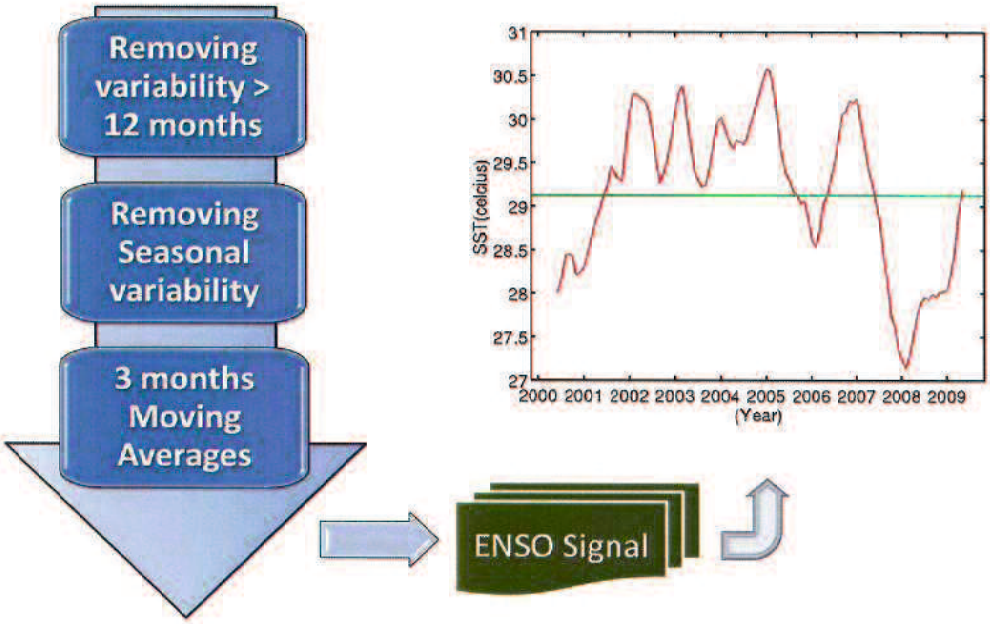

Figure 4.27. The ENSO signal detection by the proposed method on area J. The result shows the same detection of El Nino and La Nina events in the same year with NOAA index.

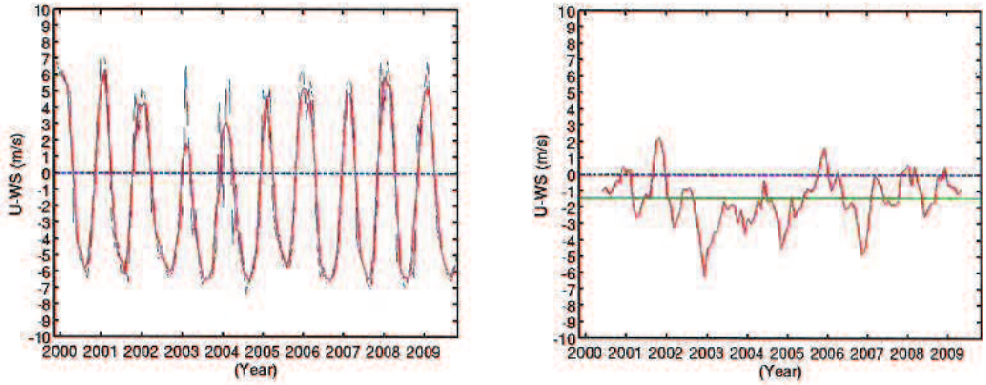

Figure 4.28. The ENSO signal detection by the proposed method on the area that shows a cyclic temporal variability. The left panel indicates the 3 months moving averages result; and the right panel indicates the result of the proposed method.

Figure 4.28 demonstrates that the proposed method is better than the 3 months moving averages of NOAA method for the areas that show a cyclic temporal variability. Based on this proposed method, we analyzed the connection of indices with the ENSO and IOD phenomena in all local areas. The results of proposed method can be shown in Figures 4.29 to 4.32. We summaries the El Nino and La Nina years in Table 4.5 and 4.6, respectively.

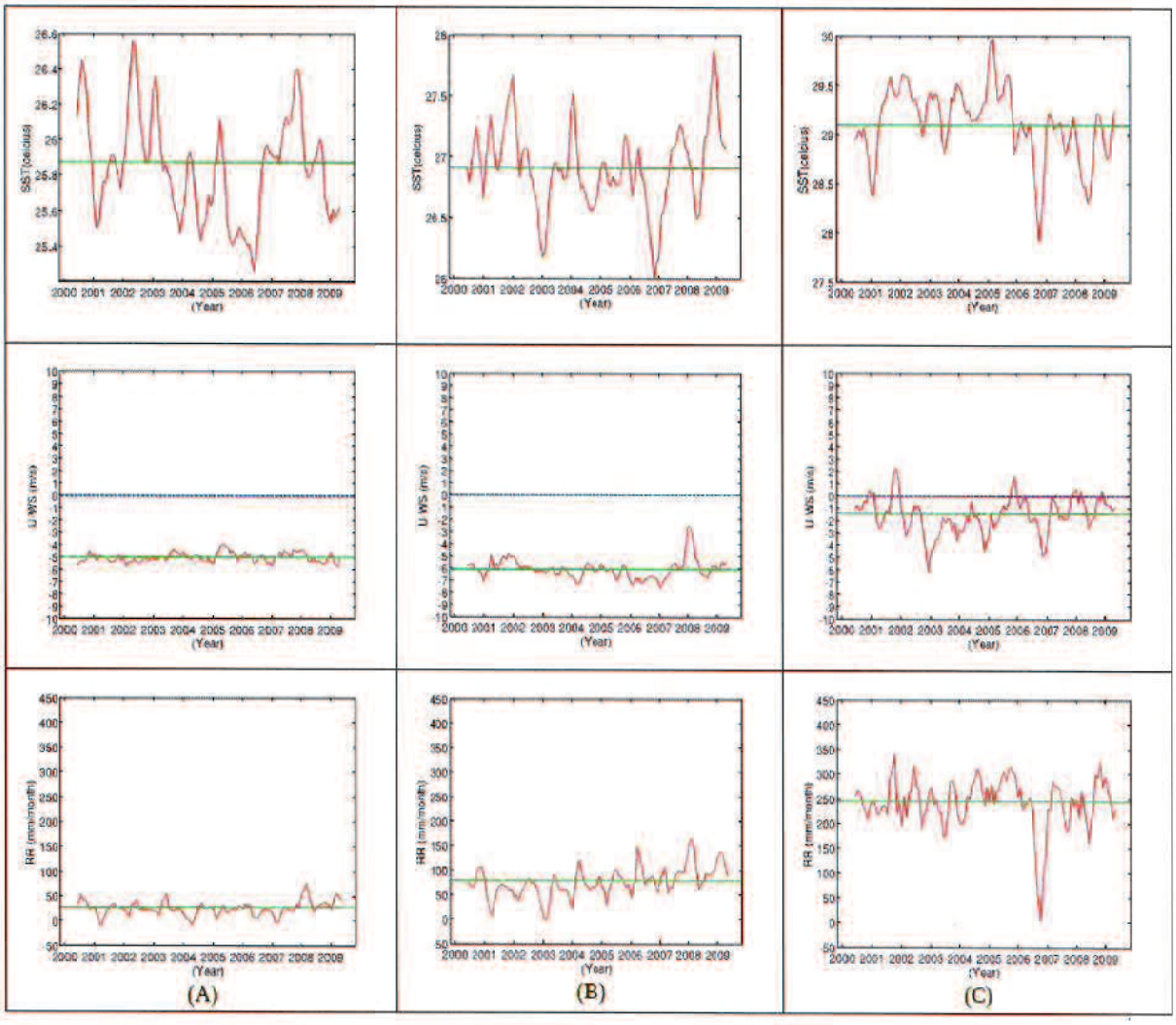

Figure 4.29. The 3 months moving averages of the deseasonalized dataset in area A (left panel), area B (middle panel) and area C (right panel). The upper panel shows the SST; the middle panel shows the UWS; and the lower panel shows the RR. The red line indicates the moving averages result and the green line indicates the average values. Axes indicate averages value of indices and year.

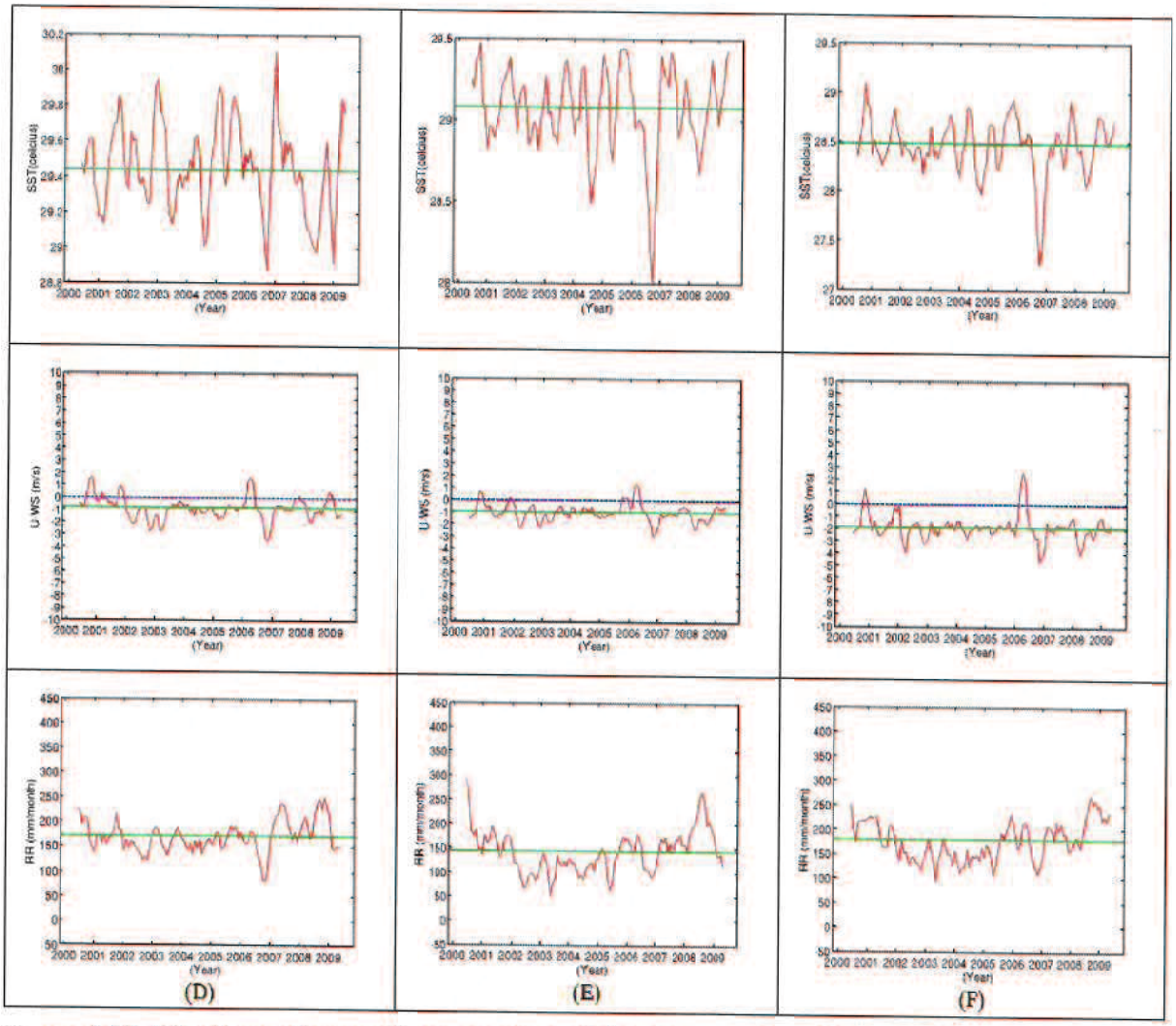

Figure 4.30. The 3 months moving averages of the deseasonalized dataset in area D (left panel), area E (middle panel) and area F (right panel). The upper panel shows the SST; the middle panel shows the UWS; and the lower panel shows the RR. The red line indicates the moving averages result and the green line indicates the average values. Axes indicate averages value of indices and year.

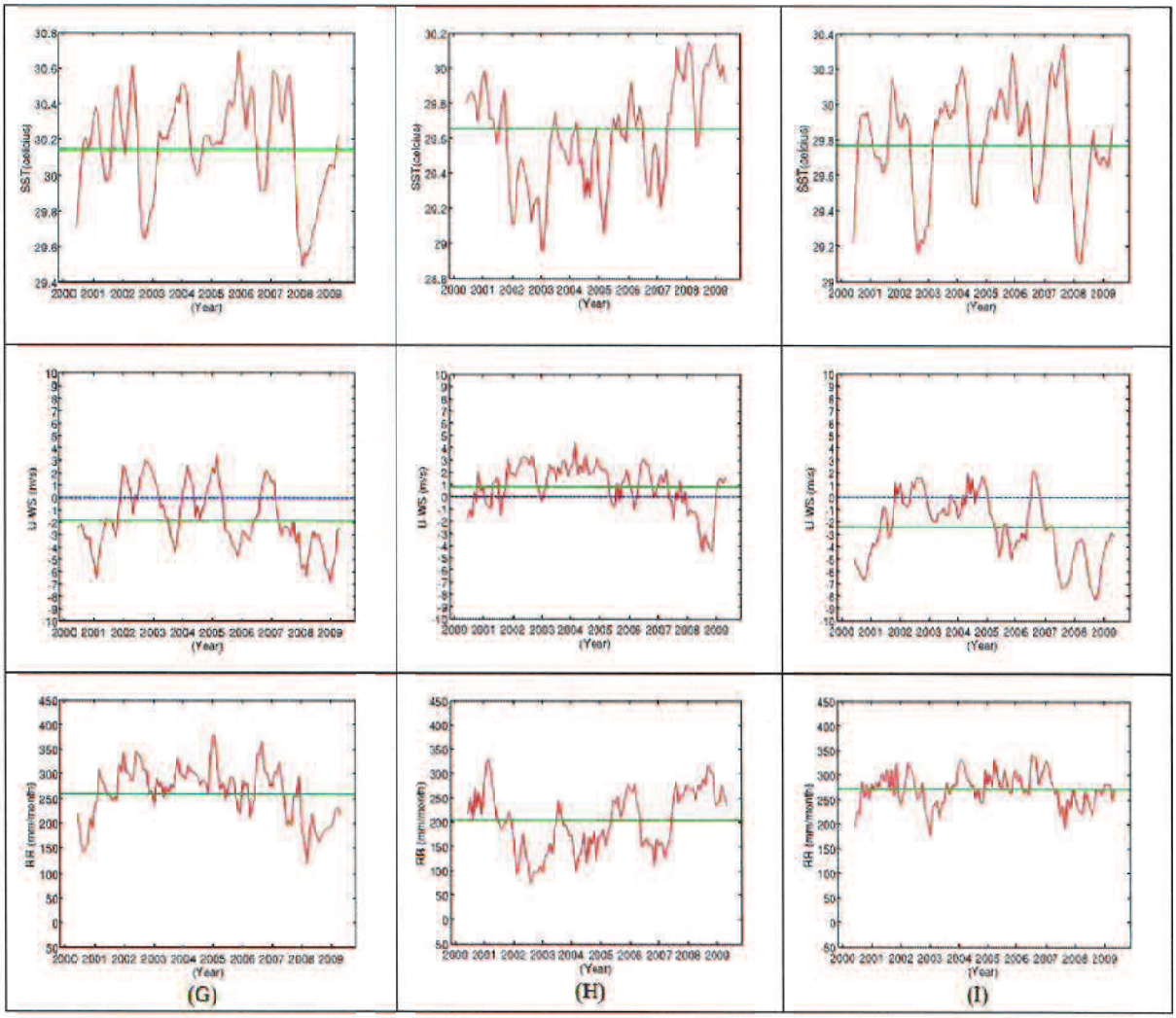

Figure 4.31. The 3 months moving averages of the deseasonalized dataset in area G (left panel), area H (middle panel) and area I (right panel). The upper panel shows the SST; the middle panel shows the UWS; and the lower panel shows the RR. The red line indicates the moving averages result and the green line indicates the average values. Axes indicate averages value of indices and year.

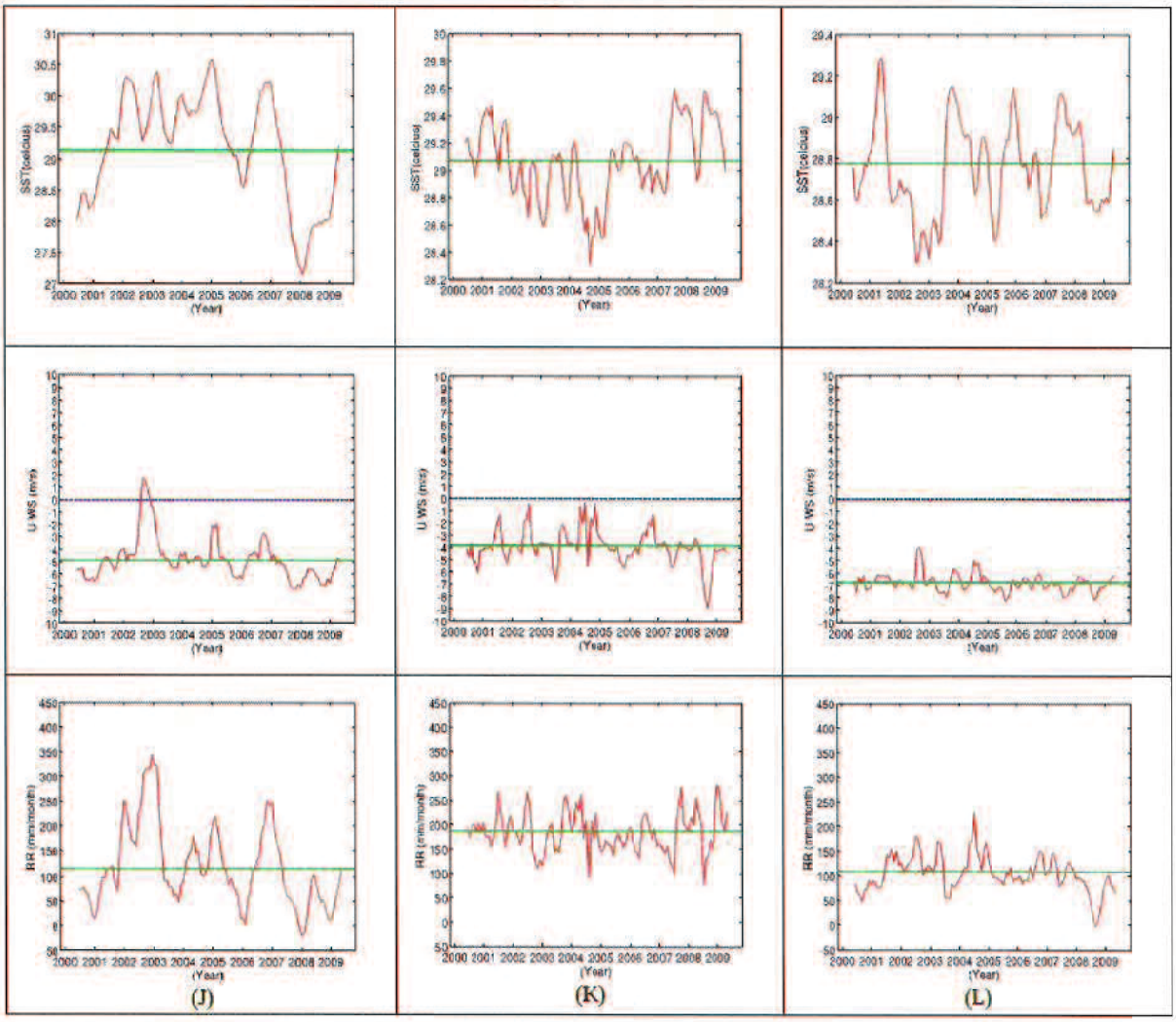

Figure 4.32. The 3 months moving averages of the deseasonalized dataset in area J (left panel), area K (middle panel) and area L (right panel). The upper panel shows the SST; the middle panel shows the UWS; and the lower panel shows the RR. The red line indicates the moving averages result and the green line indicates the average values. Axes indicate averages value of indices and year.

4.5.2 The Response of Indices to the ENSO and IOD Signals

The ENSO and IOD indices are defined as SST. We first consider the connection of SST in the Indonesian Seas with the ENSO and IOD signals (see Figure 4.33). Based on the comparison, we can discern the effect of the ENSO and IOD signals on the local areas.

Table 4.5. El Nino signal from the 3 months moving averages of the deseasonalized dataset.

Location	SST			UWS			RR		
	02/03	04/05	06/07	02/03	04/05	06/07	02/03	04/05	06/07
Area A	NC	NC	NC	NC	NC	NC	NC	D	D
Area B	D	D	D	NC	NC	NC	D	D	NC
Area C	D	D	NC	D	D	D	NC	NC	NC
Area D	NC	NC	NC	D	NC	D	D	D	D
Area E	NC	NC	D	D	NC	D	D	D	D
Area F	NC	NC	D	D	NC	D	D	D	D
Area G	D	D	D	D	D	D	D	D	D
Area H	D	D	D	D	D	D	D	D	D
Area I	D	D	D	D	D	D	D	D	D
Area J	D	D	D	D	D	D	D	D	D
Area K	D	D	NC	D	D	D	D	D	NC
Area L	D	D	D	D	D	NC	D	D	D

The D symbol indicates the signal can be detected, while NC indicates the signal is not clear.

Table 4.6. La Nina signal from the 3 months moving averages of the deseasonalized dataset.

Location	SST				UWS				RR			
	00/01	05/06	07/08	08/09	00/01	05/06	07/08	08/09	00/01	05/06	07/08	08/09
Area A	NC	NC	NC	NC	NC	NC	NC	NC	D	NC	D	D
Area B	D	D	D	D	NC	NC	NC	NC	D	NC	D	D
Area C	D	NC	D	D	D	D	D	D	NC	NC	NC	NC
Area D	NC	NC	NC	NC	D	D	D	D	D	NC	D	D
Area E	NC	NC	NC	NC	D	D	NC	NC	D	D	D	D
Area F	NC	NC	NC	NC	D	D	NC	NC	D	D	D	D
Area G	D	D	D	NC	D	D	D	D	D	NC	D	D
Area H	D	NC	D	D	D	D	D	D	D	D	D	D
Area I	NC	D	D	NC	D	D	D	D	D	NC	D	D
Area J	D	D	D	D	D	D	D	D	D	D	D	D
Area K	D	NC	D	D	D	D	D	D	NC	D	D	D
Area L	D	D	D	NC	NC	D	D	D	D	D	D	D

The D symbol indicates the signal can be detected, while NC indicates the signal is not clear.

In the Pacific Ocean, the areas H, G and I (the Equatorial region) show both El Nino and La Nina signals of SST. The areas K, B and L (the High latitude region) also show both El Nino and La Nina signals of SST.

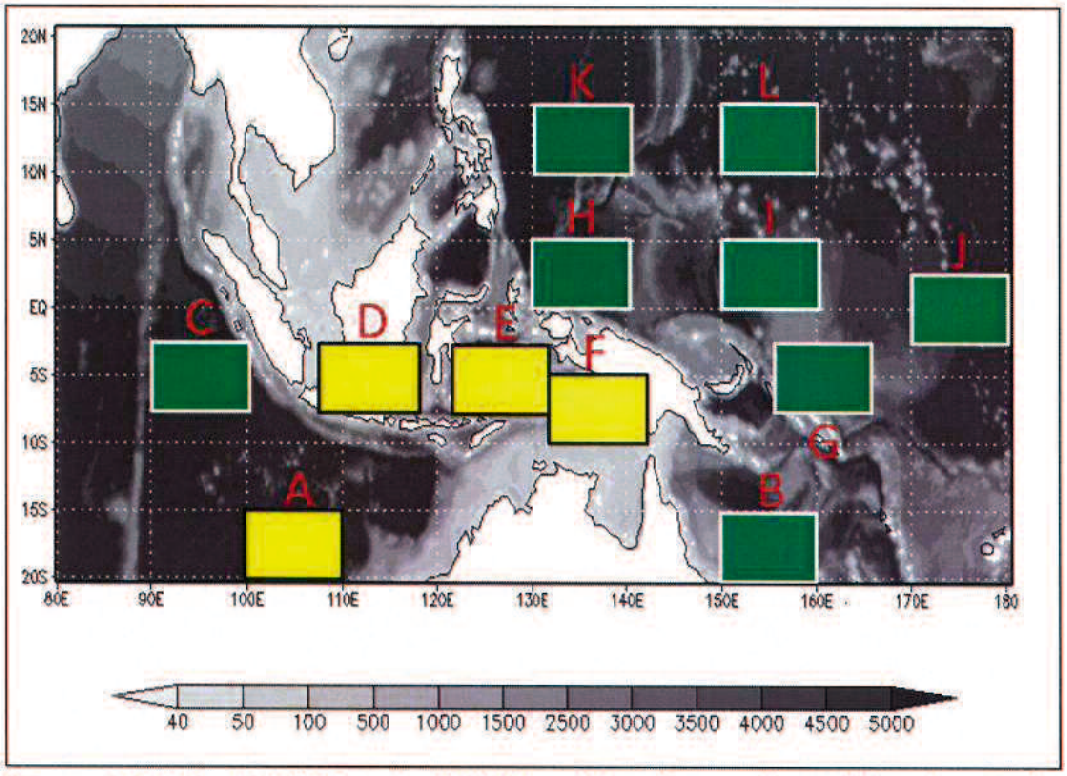

Figure 4.33. The ENSO signal of SST in all local areas. In each local area, the green colour indicates that the El Nino and La Nina signals; and the yellow colour indicates unclear ENSO signal.

In the inner Indonesian Seas, areas D, E and F, has no El Nino and no La Nina signals of SST, except for the areas E and F in the year of 2007. The abnormal signal of areas E and F in 2007 might be caused by IOD. This fact implies that the variability of SST in the areas E and F in 2007 might be caused and enhanced by the combined El Nino and IOD. The combined enhancement of La Nina and IOD might give a significant impact, but this enhancement has not occurred in our study period.

In the Indian Ocean, the area A (the High latitude region) has no El Nino and no La Nina signals of SST. The area C (the Equatorial region) shows the El Nino and La Nina signals of SST.

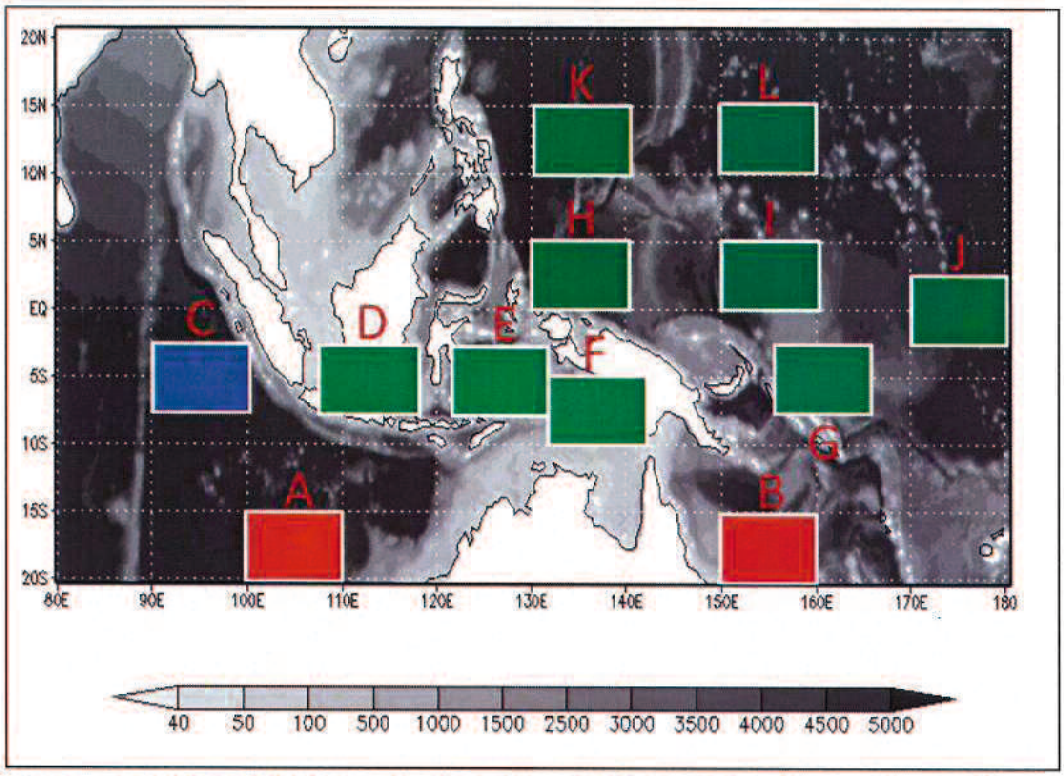

Figure 4.34. The ENSO signal of U-WS and RR in all local areas. In each local area, the red colour indicates that the ENSO signal only in RR; the blue colour indicates that the ENSO signal only in U-WS; the green colour indicates that the ENSO signal in U-WS and RR.

For the response of U-WS and RR (see Figure 4.34), the area A (the High latitude Indian Ocean) only shows the El Nino and La Nina signals of RR. The area C (the Equatorial Indian Ocean) only shows the El Nino and La Nina signals of U-WS. All areas in the High latitude Pacific Ocean show the El Nino and La Nina signals of U-WS and RR, except for the area B. The area B (the High latitude Pacific Ocean) has no El Nino and no La Nina signals of U-WS. All areas

in the Equatorial Pacific Ocean and the inner Indonesian Seas show the El Nino and La Nina signals of U-WS and RR.

4.6 The local characteristics

The inner Indonesian Seas, areas D, E and F, show the seasonal variability of all indices. However, the area D has more stable SST than the area E, while both areas have a similar U-WS pattern (see Figures 4.4 and 4.5). The difference of SST between areas D and E might be caused by the ocean bathymetry (see Figure 4.1).

The U-WS in the inner Indonesian Seas switches from west to east and vice versa (see Figures 4.4 to 4.6), while it does not change its direction in the outside areas of the inner Indonesian Seas. This is the monsoon wind pattern of the inner Indonesian Seas.

CHAPTER V

CONCLUSIONS

The local characteristics of SST, U-WS and RR in the Indonesian Seas are analyzed using satellite remote sensing datasets from December 1999 – November 2009. The seasonal variability of the indices is strong in the High latitude region and the inner Indonesian Seas. The 6 months variability of SST is weakly detected in the several areas of the Equatorial region. The inner Indonesian Seas has a strong correlation among indices, but the lag times among indices vary and we can not find out any discernment regarding them. The ENSO signal of SST can be detected in the High latitude Pacific Ocean and the Equatorial region, except for the inner Indonesian Seas. The inner Indonesian Sea only shows the ENSO signal of SST in the year 2007, but it, rather, might be caused by the positive IOD. We show the variabilities and connections of the 12 areas to the ENSO and IOD, but it is difficult to obtain any finding that fits all the areas. One typical locality is the SST difference between the areas D and E.

REFERENCES

American Meteorological Society Glossary of Meteorology (2008): Monsoon. (online), [cited 2008 March 14] available from : URL : http://amsglossary.allenpress.com/glossary.

Choudhury, A.M. (1994): A Theory for The El Nino. Trieste, Italy: International Centre for Theoretical Physics.

Chung K.P., and Siegfried D.S. (1994): On the Nature of the 1994 East Asian Summer Drought. (online), [cited 2008 March 14] available from : URL : http://csc.gallaudet.edu/monsoon/impact/drought02.html.

Diaz, H. F., M. P. Hoerling, and J. K. Eischeid (2001): ENSO variability, teleconnections and climate change, Int. J. Climatol., 21, 1845-1862.

Godfrey, J.S. (1996): The effect of the Indonesian throughflow on ocean circulation and heat exchange with the atmosphere: A review. Journal of Geophysical Research, 101, pp.12, 217-12, 237.

Gordon, A.L., Susanto, R.D. and Vranes, K. (2003): Cool Indonesian throughflow as a consequence of restricted surface layer flow. Nature, 425, 824-828.

Gordon, A., Sprintall, J., Van Aken, H.M., Susanto, D., Wijffels, S., Molcard, R., Ffield, A. (2010): Pranowo, W., Wirasantosa, S., The Indonesian throughflow during 2004-2006 as observed by the INSTANT program, Dyn. Atmos. Oceans.

I Ketut Swardika, Tasuku Tanaka and Haruma Ishida (2012): Study on the characteristics of the Indonesian Seas using satellite remote-sensing data for 1998-2007, International Journal of Remote Sensing, 33:8, 2378-2394.

International Research Institute (2013): ENSO Basics. (online), [cited 2013 March 10] available from : URL : http://iri.columbia.edu/climate/ENSO/background/basics.html.

JAMSTEC (2012): Indian Ocean Dipole. (online), [cited 2013 March 14] available from : URL : http://www.jamstec.go.jp/frsgc/research/d1/iod/e/index.html.

JAXA (2006): TRMM Data Users Handbook. (online), [cited 2013 April 5] available from : URL : http://www.eorc.jaxa.jp/TRMM/about/top_e.html.

JAXA (2007): Satellite Overview. (online), [cited 2008 April 5] available from : URL : http://www.eorc.jaxa.jp/TRMM/about/outline/outline_e.htm.

NOAA (2013): TAO Diagrams. (online), [cited 2013 March 14] available from : URL : http://www.pmel.noaa.gov/tao/proj_over/diagrams/index.html.

Orangutan Foundation International (2007): Science Corner #2: Climate of Borneo. (online) [cited 2008 May 22] available from : URL : http://www.orangutan.org/article_climate_of_borneo.php.

Pages (2008): Australasian Monsoon. (online) [cited 2008 May 22] available from : URL : http://www.pages-igbp.org/about/national/indonesia/am.html.

Remote Sensing System (2009): Description of TMI Data Products. (online), [cited 2008 March 14] available from : URL : http://www.tmi-data.com/tmi/tmi_description.html.

Saji, N. H., B. N. Goswami, P. N. Vinayachandran and T. Yamagata (1999): A dipole mode in the tropical Indian Ocean, Nature, 401, 360-363.

Saji, N. H., and T. Yamagata (2003): Possible impacts of Indian Ocean Dipole events on global climate, Climate Res., 25, 151-169.

Smith, W.H.F., Sandwell, D.T. (1997): Global seafloor topography from satellite altimetry and ship depth soundings, Science 277, 1957-1962.

Sprintall, J., Susan, W., Gordon, A.L., Amy, F.R., Molcard, R., Susanto, D., Indroyono, S., Sopaheluwakan, J., Yusuf, S., van Aken, H.M. (2004): INSTANT: A New International Array to Measure the Indonesian Throughflow, Eos 85 No.39, 369-376.

Teresa Z. (2008): Dive Sites in Indonesia. (online), [cited 2008 Jun. 4 at 08:27] available from : URL : http://www.starfish.ch/dive/Indonesia.

Trenberth, K. E., G. W. Branstator, D. Karoly, A. Kumar, N.-C. Lau, C. Ropelewski (1998): Progress during TOGA in understanding and modeling global teleconnections associated with tropical sea surface temperatures, J. Geophys. Res., 103(C7), 14291-14324, 10.1029/97JC01444.

Tropical Atmosphere Ocean (2013): What is an El Niño? [cited 2013 March 14] available from: URL : http://www.pmel.noaa.gov/tao/elnino/el-nino-story .html